PHYSICAL REVIEW D **85,** 124032 (2012)

Numerical stability of the Z4c formulation of general relativity

Zhoujian Cao[1] and David Hilditch[2]

[1]*Institute of Applied Mathematics, Academy of Mathematics and Systems Science, Chinese Academy of Sciences, Beijing 100190, China*

[2]*Theoretical Physics Institute, University of Jena, 07743 Jena, Germany*

(Received 10 November 2011; published 18 June 2012)

We study numerical stability of different approaches to the discretization of a conformal decomposition of the Z4 formulation of general relativity. We demonstrate that in the linear, constant coefficient regime a novel discretization for tensors is formally numerically stable with a method of lines time integrator. We then perform a full set of "*apples with apples*" tests on the nonlinear system, and thus present numerical evidence that both the new and standard discretizations are, in some sense, numerically stable in the nonlinear regime. The results of the Z4c numerical tests are compared with those of Baumgarte-Shapiro-Shibata-Nakamura-Oohara-Kojima (BSSNOK) evolutions. We typically do not employ the Z4c constraint damping scheme and find that in the robust stability and gauge wave tests the Z4c evolutions result in lower constraint violation at the same resolution as the BSSNOK evolutions. In the gauge wave tests, we find that the Z4c evolutions maintain the desired convergence factor over many more light-crossing times than the BSSNOK tests. The difference in the remaining tests is marginal.

DOI: 10.1103/PhysRevD.85.124032 PACS numbers: 04.25.D−, 95.30.Sf

I. INTRODUCTION

There are currently two main formulations used in the numerical evolution of astrophysically interesting spacetimes by the methods of numerical relativity. The first was pioneered by Pretorius [1,2] and later adopted by other numerical relativity groups, for example [3–5]. In this approach the generalized harmonic gauge (GHG) formulation of general relativity [6,7] is employed with black-hole excision. That is, inside the black-hole horizon the numerical mesh contains a "cut-out" region. The generalized harmonic formulation has a number of desirable properties. The first is that it has a trivially wavelike principal part, which allows the construction of boundary conditions that lead to a well-posed initial boundary value problem that can be implemented numerically [3,8–14]. That the wavelike nature of the formulation is inherited by the constraint subsystem means that these boundary conditions can conveniently be made constraint preserving, and that when numerical error causes violations of the constraints, this violation may propagate off of the numerical grid, hopefully to be harmlessly absorbed by the aforementioned boundary conditions. The evolution system also admits a constraint damping scheme [15], which has proven important in numerical applications to avoid constraint violating blowups. The second main formulation is the combination of the Baumgarte-Shapiro-Shibata-Nakamura-Oohara-Kojima (BSSNOK) system [16–18], the moving puncture family of gauge conditions, and puncture black-hole initial data [19,20]. Using this method coordinate singularities, or punctures, are explicitly advected across the numerical mesh. The puncture method has proven extremely robust in the evolution of even extreme initial data [21,22]. But on the other hand, while well posedness for the initial value problem of BSSNOK with suitable members of the puncture gauge family has been established [23] the complicated structure of the principal part has prevented the same development of boundary conditions for the system, although interesting progress has been made [24].

This status begs the question: is it possible to write down a formulation with the strengths of both GHG and BSSNOK for numerical applications? In [25] a natural candidate, namely a conformal decomposition of the Z4 formulation [26–32], Z4c was identified, and indeed found to give favorable results over those of BSSNOK in the context of spherical symmetry. Like that of GHG, the constraint subsystem of the Z4 formulation has a trivial wavelike principal part. This structure is inherited by the constraint subsystem of the conformally decomposed system provided that the additional constraints introduced by the decomposition are explicitly imposed. This property allows the convenient construction of constraint preserving boundary conditions for the Z4c system [33]. The Z4c system furthermore inherits the constraint damping scheme of Z4, which was studied in detail in [34]. So far the numerical studies of Z4c have been restricted to spherical symmetry. Recently, a variant of the conformal decomposition, CCZ4, was performed, and for the first time numerical evolutions in three dimensions were presented [35]. The difference between Z4c and CCZ4 is that in the conformal decomposition of Z4c nonprincipal constraint additions are discarded in such a way to make the resulting evolution system as close as possible to BSSNOK. On the other hand in CCZ4 no constraint terms are discarded. Therefore the two formulations share the same principal part, and thus the same basic partial differential equation (PDE) properties. Now that there is robust evidence in favor of the Z4c system in spherical symmetry, we also

turn our attention to three spatial dimensions. Since there is a wealth of experience concerning the robustness of the GHG and BSSNOK formulations in applications, significant evidence must be presented that an alternative formulation is competitive, and we therefore take a conservative approach, and focus here on the question of numerical stability.

In Sec. II we present the equations of motion of the Z4c system and the gauge conditions that we employ in both our analytical and numerical studies. In Sec. III we introduce a novel discretization of tensors and show that in the linear constant coefficient approximation Z4c, coupled to the puncture gauge, is numerically stable with this discretization and a method of lines time integrator. In Sec. IV we present a complete set of "*apples with apples*" tests for the Z4c formulation. In Appendices A and B we discuss hyperbolicity of the conformal decomposition without imposition of the algebraic constraints, and symmetric hyperbolicity of the formulation with the puncture gauge. We conclude in Sec. V.

II. THE Z4C FORMULATION

The Z4 formulation [26], with constraint damping [15] replaces the Einstein field equations $G_{ab} = 8\pi T_{ab}$ by

$$G_{ab} = 8\pi T_{ab} - \nabla_a Z_b - \nabla_b Z_a + g_{ab}\nabla_c Z^c + \kappa_1[n_a Z_b + n_b Z_a + \kappa_2 g_{ab} n_c Z^c], \quad (1)$$

where $G_{ab} = R_{ab} - \frac{1}{2}R g_{ab}$ is the Einstein tensor while R_{ab} is the Ricci tensor, ∇_a is the covariant derivative operator compatible with g_{ab}, and Z_a is an additional vector field of constraints. Under the standard $3+1$ decomposition, against a timelike unit normal vector n^a, defining $\Theta \equiv -n^a Z_a$ and $Z_i \equiv \perp_i^a Z_a$ one finds the expressions given in [15]. If the spacetime is without boundary and does not admit a Killing vector, it can be shown that if the constraints are satisfied in one spacelike slice then they will vanish at all times [26]. We may therefore take a free-evolution approach to the problem. For PDEs and numerical analysis we work in the expanded phase space, in which the constraints may be violated. In numerical applications the constraints are to be solved for initial data, and their compatibility with the evolution equations means that any violation should converge away with resolution.

From the PDEs point of view, only the principal derivative additions can affect well posedness of the initial value problem of the formulation as a PDE system. In order to make a conformal decomposition we therefore discard nonprincipal terms in such a way that the resulting equations of motion will have a form similar to those of the BSSNOK formulation when written in terms of conformal variables. Of course we keep the constraint damping terms. The Z4c formulation equations of motion [25,33] are

$$\partial_t \gamma_{ij} = -2\alpha K_{ij} + \mathcal{L}_\beta \gamma_{ij}, \quad (2)$$

$$\partial_t K_{ij} = -D_i D_j \alpha + \alpha[R_{ij} + K K_{ij} - 2K_{ik}K^k{}_j + 2\hat{D}_{(i}Z_{j)} - \kappa_1(1+\kappa_2)\Theta\gamma_{ij}] + 4\pi\alpha[\gamma_{ij}(S - \rho_{\mathrm{ADM}}) - 2S_{ij}] + \mathcal{L}_\beta K_{ij}, \quad (3)$$

for the metric and extrinsic curvature, and

$$\partial_t \Theta = \tfrac{1}{2}\alpha[H + 2\hat{D}^i Z_i - 2\kappa_1(2+\kappa_2)\Theta] + \mathcal{L}_\beta \Theta, \quad (4)$$

$$\partial_t Z_i = \alpha[M_i + D_i\Theta - \kappa_1 Z_i] + \gamma^{1/3} Z^j \partial_t[\gamma^{-(1/3)}\gamma_{ij}] + \beta^j \hat{D}_j Z_i, \quad (5)$$

for the constraints Θ and Z_i, where here we define

$$\hat{D}_i Z_j = \gamma^{1/3}\gamma_{kj}\partial_i[\gamma^{-(1/3)}Z^k], \quad (6)$$

and use the shorthands

$$H = R - K_{ij}K^{ij} + K^2 - 16\pi\rho_{\mathrm{ADM}}, \quad (7)$$

$$M_i = D^j[K_{ij} - \gamma_{ij}K] - 8\pi S_i, \quad (8)$$

for the Hamiltonian and momentum constraints. Similar to the conformal transformation made in the BSSNOK formalism, we introduce conformal variables,

$$\tilde{\gamma}_{ij} = \gamma^{-1/3}\gamma_{ij}, \qquad \chi = \gamma^{-1/3}, \quad (9)$$

$$\tilde{A}_{ij} = \gamma^{-1/3}(K_{ij} - \tfrac{1}{3}\gamma_{ij}K), \qquad \hat{K} = K - 2\Theta, \quad (10)$$

$$\tilde{\Gamma}^i = 2\tilde{\gamma}^{ij}Z_j + \tilde{\gamma}^{ij}\tilde{\gamma}^{kl}\tilde{\gamma}_{jk,l}, \qquad \tilde{\Gamma}_{\mathrm{d}}{}^i = \tilde{\Gamma}^i{}_{jk}\tilde{\gamma}^{jk}. \quad (11)$$

Under this change of variables the evolution equations become

$$\partial_t \chi = \tfrac{2}{3}\chi[\alpha(\hat{K} + 2\Theta) - D_i\beta^i], \quad (12)$$

$$\partial_t \tilde{\gamma}_{ij} = -2\alpha\tilde{A}_{ij} + 2\tilde{\gamma}_{k(i}\partial_{j)}\beta^k - \tfrac{2}{3}\tilde{\gamma}_{ij}\partial_k\beta^k + \beta^k\partial_k\tilde{\gamma}_{ij}, \quad (13)$$

$$\partial_t \hat{K} = -D_i D^i\alpha + \alpha[\tilde{A}_{ij}\tilde{A}^{ij} + \tfrac{1}{3}(\hat{K} + 2\Theta)^2 + \kappa_1(1 - \kappa_2)\Theta] + 4\pi\alpha[S + \rho_{\mathrm{ADM}}] + \beta^i\partial_i\hat{K}, \quad (14)$$

$$\partial_t \tilde{A}_{ij} = \chi[-D_i D_j\alpha + \alpha(R_{ij} - 8\pi S_{ij})]^{\mathrm{tf}} + \alpha[(\hat{K} + 2\Theta)\tilde{A}_{ij} - 2\tilde{A}_{ik}\tilde{A}^k{}_j] + 2\tilde{A}_{k(i}\partial_{j)}\beta^k - \tfrac{2}{3}\tilde{A}_{ij}\partial_k\beta^k + \beta^k\partial_k\tilde{A}_{ij}, \quad (15)$$

$$\partial_t \Theta = \tfrac{1}{2}\alpha[R - \tilde{A}_{ij}\tilde{A}^{ij} + \tfrac{2}{3}(\hat{K} + 2\Theta)^2 - 16\pi\rho_{\mathrm{ADM}} - 2\kappa_1(2+\kappa_2)\Theta] + \beta^i\partial_i\Theta, \quad (16)$$

$$\partial_t \tilde{\Gamma}^i = \tilde{\gamma}^{jk}\partial_j\partial_k\beta^i + \tfrac{1}{3}\tilde{\gamma}^{ij}\partial_j\partial_k\beta^k - 2\tilde{A}^{ij}\partial_j\alpha + 2\alpha[\tilde{\Gamma}^i{}_{jk}\tilde{A}^{jk} - \tfrac{3}{2}\tilde{A}^{ij}\partial_j \ln\chi - \tfrac{1}{3}\tilde{\gamma}^{ij}\partial_j(2\hat{K}+\Theta) - \kappa_1(\tilde{\Gamma}^i - \tilde{\Gamma}_{\rm d}{}^i) - 8\pi\tilde{\gamma}^{ij}S_j] + \tfrac{2}{3}\tilde{\Gamma}_{\rm d}{}^i\partial_j\beta^j - \tilde{\Gamma}_{\rm d}{}^j\partial_j\beta^i + \beta^j\partial_j\tilde{\Gamma}^i, \quad (17)$$

where we absorb the constraint addition into the Ricci tensor according to

$$R_{ij} = R^{\chi}{}_{ij} + \tilde{R}_{ij}, \quad (18)$$

$$\tilde{R}^{\chi}{}_{ij} = \frac{1}{2\chi}\tilde{D}_i\tilde{D}_j\chi + \frac{1}{2\chi}\tilde{\gamma}_{ij}\tilde{D}^l\tilde{D}_l\chi - \frac{1}{4\chi^2}\tilde{D}_i\chi\tilde{D}_j\chi - \frac{3}{4\chi^2}\tilde{\gamma}_{ij}\tilde{D}^l\chi\tilde{D}_l\chi, \quad (19)$$

$$\tilde{R}_{ij} = -\tfrac{1}{2}\tilde{\gamma}^{lm}\tilde{\gamma}_{ij,lm} + \tilde{\gamma}_{k(i}\partial_{j)}\tilde{\Gamma}^k + \tilde{\Gamma}_d{}^k\tilde{\Gamma}_{(ij)k} + \tilde{\gamma}^{lm}(2\tilde{\Gamma}^k{}_{l(i}\tilde{\Gamma}_{j)km} + \tilde{\Gamma}^k{}_{im}\tilde{\Gamma}_{klj}). \quad (20)$$

In this study we consider only vacuum spacetimes, so S_{ij}, S_i, and $\rho_{\rm ADM}$ all vanish. Note that the conformal decomposition introduces two algebraic constraints,

$$D \equiv \ln\det\tilde{\gamma} = 0, \qquad T \equiv \gamma^{ij}\tilde{A}_{ij} = 0, \quad (21)$$

to the system. In our numerical experiments they are imposed explicitly after every time step. If the constraint projection is not performed then one is performing free evolution in the larger phase space in which the algebraic constraints are violated, meaning that the PDE properties of the system must be reevaluated. We close the system with the puncture gauge condition, which consists of the Bona-Másso lapse [36] and the gamma-driver shift conditions [37],

$$\partial_t\alpha = -\mu_L\alpha^2\hat{K} + \beta^i\partial_i\alpha, \quad (22)$$

$$\partial_t\beta^i = \mu_S\alpha^2\tilde{\Gamma}^i - \eta\beta^i + \beta^j\partial_j\beta^i. \quad (23)$$

When coupled to the puncture gauge the Z4c formulation forms a PDE system that is generically strongly hyperbolic. In our numerical applications we almost always take the "1 + log" variant of the lapse condition $\mu_L = 2/\alpha$ and $\mu_S = 1/\alpha^2$, although some tests are performed with harmonic lapse $\mu_L = 1$. The shift damping term η is chosen according to the needs of the numerical test. We also sometimes employ the harmonic shift condition,

$$\partial_t\beta^i = \alpha^2[\chi\tilde{\Gamma}^i + \tfrac{1}{2}\chi\tilde{\gamma}^{ij}\chi_{,j} - \chi\tilde{\gamma}^{ij}\partial_j\ln\alpha] + \beta^j\partial_j\beta^i. \quad (24)$$

III. NUMERICAL STABILITY

In this section we demonstrate that when coupled to the puncture gauge and linearized around the Minkowski spacetime, the Z4 formulation is numerically stable with a particular discretization. The calculations build on studies of numerical stability for first order in time, second order in space systems [38–40], and essentially rely on the theory of [41,42].

A. A novel discretization of second order systems of tensors

1. Motivation

For linear, constant coefficient first order strongly hyperbolic systems, strong hyperbolicity is enough to guarantee numerical stability under a method of lines approach, which is no longer the case for first order in time, second order in space systems. If in addition to being strongly hyperbolic, the PDE system is symmetric hyperbolic, then a discrete energy method can be used to guarantee numerical stability. There are many second order PDE systems of interest that are only strongly hyperbolic, for which other methods must be used in analysis. Unfortunately, when using the standard discretization in space for strongly hyperbolic second order systems it is often not even possible to analyze whether or not the resulting semidiscrete system is stable with computer algebra. The reason for this is that there is not a straightforward relationship between the principal symbol of the semidiscrete system and that of the continuum; various sectors of the principal symbol that are decoupled at the continuum become entangled in the semidiscrete system. Here we present a novel discretization for systems of tensors for which semidiscrete stability analysis can at least be tackled. Intuitively this is made possible because after Fourier transform the novel discretization has only one wave vector, whereas the standard discretization has two. The novel discretization does not guarantee numerical stability whenever the continuum system is strongly hyperbolic. Therefore the situation is still not entirely satisfactory.

2. The standard discretization

For a grid-function f, where here and in the following we suppress indices labeling the position on the grid, the standard second order discretization accurate for second order in space systems is

$$\partial_i \to D_{0i}, \qquad \partial_i\partial_j \to \begin{cases} D_{0i}D_{0j} & \text{if } i \neq j, \\ D_{+i}D_{-i} & \text{if } i = j, \end{cases} \quad (25)$$

where we use the standard notation for centered and one-sided finite difference operators. The standard fourth order accurate discretization for second order in space systems is

$$\partial_i \to D_i^{(4)} \equiv D_{0i}\left(1 - \frac{h^2}{6}D_{+i}D_{-i}\right),$$
$$\partial_i\partial_j \to D_{0i}^{(4)} \equiv \begin{cases} D_{0i}^{(4)}D_{0j}^{(4)} & \text{if } i \neq j, \\ D_{+i}D_{-i}\left(1 - \frac{h^2}{12}D_{+i}D_{-i}\right) & \text{if } i = j, \end{cases} \quad (26)$$

where here we drop the summation convention. This approach to discretization can of course be naturally extended to higher order accuracy.

3. A novel approach to the discretization of tensors

We are concerned with numerical approximations to the spatial derivatives of scalars, vectors, and symmetric two-tensors, and assume that we have a metric δ_{ij} in space. Suppose that we are given the finite difference approximations $D^{(1)}_i$ and $D^{(2)}_{ij}$ to the first and second derivatives, respectively. In concrete terms we mean by this either the standard second (25) or fourth order accurate discretization (26) above. In each of these discretizations the symmetry is used to reduce the size of the stencil for second derivatives $\partial_i\partial_j$ with $i = j$, meaning that the approximation of the second derivative is not equivalent to repeated application of the approximation of the first. For the first derivative we must always use $D^{(1)}_i$. On the other hand, for second derivatives we may sometimes use repeated application of $D^{(1)}_i$, and sometimes $D^{(2)}_{ij}$. We choose to approximate the Laplace operator by

$$\eta^{ij}\partial_i\partial_j \rightarrow \Delta^{(2)} \equiv \eta^{ij}D^{(2)}_{ij}. \tag{27}$$

Second gradients of scalars are approximated by

$$\partial_i\partial_j u \rightarrow [D^{(1)}_i D^{(1)}_j]^{\mathrm{tf}} u + \tfrac{1}{3}\delta_{ij}\Delta^{(2)}u. \tag{28}$$

For vectors we distinguish gradient-divergence terms by using repeated application of the first derivative,

$$\partial_i\partial_j f^j \rightarrow D^{(1)}_i D^{(1)}_j f^j. \tag{29}$$

Likewise, for symmetric two-tensors we approximate divergence-divergence terms by repeated application of the first derivative approximation, although such terms do not appear in our applications. In [38] numerical stability of a parametrized generalization of the Knapp-Walker-Baumgarte formulation [43] of electromagnetism was discussed. It was found that with the standard discretization there are choices of the formulation parameter that render the system numerically unstable, despite the initial value problem being well posed at the continuum. It is straightforward to show that with the novel discretization, using the standard second order discretization for the raw approximation, the semidiscrete system is numerically stable for all choices of the parameters that render the initial value problem well posed.

B. Application to the Z4 formulation

1. The linearized system

In this section we present the Z4c field equations linearized around the line element,

$$\mathrm{d}s^2 = -\mathrm{d}t^2 + \delta_{ij}\mathrm{d}x^i\mathrm{d}x^j, \tag{30}$$

where we denote the constant, with respect to both space and time, background spatial metric by δ_{ij}. The background shift, extrinsic curvature, and Z4 constraints are taken to vanish. We denote the perturbations by α, β^i, γ_{ij}, Θ, Z_i, K_{ij}. The linearized equations of motion are

$$\partial_t\gamma_{ij} = -2K_{ij} + 2\partial_{(i}\beta_{j)}, \tag{31}$$

$$\partial_t\alpha = -\mu_L(K - 2\Theta), \tag{32}$$

$$\partial_t\beta^i = \bar{\mu}_S f^i, \tag{33}$$

$$\partial_t K_{ij} = -\tfrac{1}{2}\partial^k\partial_k\gamma_{ij} - \tfrac{1}{6}\partial_i\partial_j\gamma - \partial_i\partial_j\alpha + \partial_{(i}f_{j)}, \tag{34}$$

$$\partial_t\Theta = -\tfrac{1}{3}\partial^i\partial_i\gamma + \tfrac{1}{2}\partial_i f^i, \tag{35}$$

$$\partial_t f^i = \partial^j\partial_j\beta^i + \tfrac{1}{3}\partial_i\partial_j\beta^j - \tfrac{4}{3}\partial^i K + 2\partial^i\Theta, \tag{36}$$

where here we have defined $\bar{\mu}_S = (\delta)^{1/3}\mu_S$, and used the Nagy-Ortiz-Reula (NOR) [44] variable

$$f^i = 2Z^i + \delta^{ij}\delta^{kl}[\partial_k\gamma_{lj} - \tfrac{1}{3}\partial_j\gamma_{kl}]. \tag{37}$$

The linearized Hamiltonian and momentum constraints are

$$H = \partial^i\partial^j\gamma_{ij} - \partial^i\partial_i\gamma, \tag{38}$$

$$M_i = \partial^j K_{ij} - \partial_i K. \tag{39}$$

2. The semidiscrete system

We now discretize the system in space but leave time continuous. Using the novel discretization described in Sec. III A we write the system as

$$\partial_t\gamma_{ij} = -2K_{ij} + 2D^{(1)}{}_{(i}\beta_{j)}, \tag{40}$$

$$\partial_t\alpha = -\mu_L(K - 2\Theta), \tag{41}$$

$$\partial_t\beta^i = \bar{\mu}_S f^i, \tag{42}$$

$$\begin{aligned}\partial_t K_{ij} = {} & -\tfrac{1}{2}\Delta^{(2)}\gamma_{ij} - \tfrac{1}{6}[[D^{(1)}{}_i D^{(1)}{}_j]^{\mathrm{tf}} + \tfrac{1}{3}\delta_{ij}\Delta^{(2)}]\gamma \\ & - [[D^{(1)}{}_i D^{(1)}{}_j]^{\mathrm{tf}} + \tfrac{1}{3}\delta_{ij}\Delta^{(2)}]\alpha + D^{(1)}{}_{(i}f_{j)},\end{aligned} \tag{43}$$

$$\partial_t\Theta = -\tfrac{1}{3}\Delta^{(2)}\gamma + \tfrac{1}{2}D^{(1)}{}_i f^i, \tag{44}$$

$$\partial_t f^i = \Delta^{(2)}\beta^i + \tfrac{1}{3}D^{(1)i}D^{(1)}{}_j\beta^j - \tfrac{4}{3}D^{(1)i}K + 2D^{(1)i}\Theta, \tag{45}$$

where we suppress indices labeling the grid, which we take to be

$$x_i = (x_{i_1}, y_{i_2}, z_{i_3}) = (i_1 h, i_2 h, i_3 h), \tag{46}$$

with $i_i = 0, \ldots, N-1$, $h = \frac{2\pi}{N}$ the spatial resolution, and restrict our attention to 2π-periodic solutions. Note that in contrast to the continuum system the constraint subsystem does not close for the semidiscrete system. It is not obvious

how to achieve closure of the constraint subsystem at the semidiscrete level without using a "$(D_0)^2$" type discretization. Unfortunately, as discussed in [38] the D_0 norm is not strong enough for analytic considerations, and we therefore do not consider it further here.

3. Pseudodiscrete reduction to first order

Performing a discrete Fourier transform in space, defining

$$\Omega_+^2 = \sum_{i=1}^{3} |\tilde{D}_{+i}|^2, \tag{47}$$

and $\xi_i = -\pi + 2\pi/N, \ldots, -\pi + 4\pi/N + \pi$, for $i = 1, 2, 3$, and then introducing the convenient reduction variables

$$\tilde{\epsilon} = i\Omega_+ \tilde{\alpha}, \qquad \tilde{\phi}^i = i\Omega_+ \tilde{\beta}^i, \qquad \tilde{\iota}_{ij} = i\Omega_+ \tilde{\gamma}_{ij}, \tag{48}$$

results in a large set of ordinary differential equations which can be written as

$$\partial_t \tilde{\gamma}_{ij} = -2\tilde{K}_{ij} + \frac{2s}{\Omega_+} \hat{s}_{(i}\tilde{\phi}_{j)}, \tag{49}$$

$$\partial_t \tilde{\alpha} = -\mu_L(\tilde{K} - 2\tilde{\Theta}), \tag{50}$$

$$\partial_t \tilde{\beta}^i = \bar{\mu}_S \tilde{f}^i, \tag{51}$$

for the metric components,

$$\partial_t \tilde{\iota}_{ij} = -2i\Omega_+ \tilde{K}_{ij} + 2is\hat{s}_{(i}\tilde{\phi}_{j)}, \tag{52}$$

$$\partial_t \tilde{\epsilon} = -i\Omega_+ \mu_L(\tilde{K} - 2\tilde{\Theta}), \tag{53}$$

$$\partial_t \tilde{\phi}^i = i\Omega_+ \bar{\mu}_S \tilde{f}^i, \tag{54}$$

for the reduction variables, and finally

$$\partial_t \tilde{K}_{ij} = -\frac{i}{\Omega_+}\left[s^2[\hat{s}_i\hat{s}_j]^{\mathrm{tf}} + \frac{1}{3}\delta_{ij}\Omega^2\right]\tilde{\epsilon} - \frac{i}{2}\frac{\Omega^2}{\Omega_+}\tilde{\iota}_{ij} - \frac{i}{6\Omega_+}\left[s^2[\hat{s}_i\hat{s}_j]^{\mathrm{tf}} + \frac{1}{3}\delta_{ij}\Omega^2\right]\tilde{\iota} + is\hat{s}_{(i}\tilde{f}_{j)}, \tag{55}$$

$$\partial_t \tilde{\Theta} = -\frac{i}{3}\frac{\Omega^2}{\Omega_+}\tilde{\iota} + \frac{1}{2}is\tilde{f}^{\hat{s}}, \tag{56}$$

$$\partial_t \tilde{f}^i = i\frac{\Omega^2}{\Omega_+}\tilde{\phi}^i + \frac{i}{3}\frac{s^2}{\Omega_+}\hat{s}^i\tilde{\phi}^{\hat{s}} - \frac{4}{3}is\hat{s}^i\tilde{K} + 2is\hat{s}^i\tilde{\Theta}, \tag{57}$$

for the remaining quantities. Here we have defined

$$s_i = -i\tilde{D}_i^{(1)}, \quad \Omega^2 = -\tilde{\Delta}^{(2)}, \quad s^2 = s_i s^i, \quad \hat{s}^i = \frac{s^i}{s}, \tag{58}$$

and use an index $\hat{s}$ to denote contraction with the unit wave vector $\hat{s}^i$. The Fourier transformed differencing operator D_{+i} is denoted $\tilde{D}_{+i}$, and we have that

$$\tilde{D}_{+i} = \frac{2}{h} i \sin\frac{\xi_i}{2}. \tag{59}$$

Whilst estimating the growth of the solutions we may discard the nonprincipal terms because for the standard second and fourth order accurate discretizations the nonprincipal additions are bounded (Theorem 5.1.2 [42]). Note that for both the standard second and fourth order accurate discretizations we have the properties,

$$0 \le \frac{s}{\Omega} \le a, \qquad b^{-1} \le \frac{\Omega}{\Omega_+} \le b, \tag{60}$$

for some positive constants a, b, which we will use in the following. Up to nonprincipal terms the evolution of the metric components $\tilde{\alpha}$, $\tilde{\beta}^i$, $\tilde{\gamma}_{ij}$ is trivial, so they may be discarded in the following discussion. Defining the unit wave vector $\hat{s}_i$, and using it with δ_{ij} as a metric in Fourier space to perform a $2+1$ decomposition reveals that, under the novel discretization the principal symbol of the pseudodiscrete reduction decouples into a scalar $(\tilde{\iota}_{ss}, \tilde{\iota}_{qq}, \tilde{\epsilon}, \tilde{f}^s, \tilde{\hat{K}}_{ss}, \tilde{\hat{K}}_{qq}, \tilde{\Theta}, \tilde{\phi}^s)$, vector $(\tilde{\iota}_{sA}, \tilde{f}^A, \tilde{\hat{K}}_{sA}, \tilde{\phi}^A)$, and tensor $(\tilde{\iota}^{\mathrm{TF}}_{AB}, \tilde{\hat{K}}^{\mathrm{TF}}_{AB})$ sector, just like in the continuum PDEs analysis; see, for example, Sec. D of [33].

4. Characteristic variables

Each of the three sectors generically admits a complete set of characteristic variables. In the scalar sector they are

$$u_{\pm\sqrt{\mu_L}} = \frac{\Omega}{\Omega_+}\tilde{\epsilon} \pm \sqrt{\mu_L}\tilde{\hat{K}}, \tag{61}$$

which are associated with the lapse gauge condition, propagating with speed $\pm\sqrt{\mu_L}i\Omega$, and appear almost identically at the continuum level. For brevity we use the shorthands $\tilde{\hat{K}} = \tilde{K}_{\hat{s}\hat{s}} + \tilde{K}_{qq} - 2\tilde{\Theta}$ and $\tilde{\Lambda} = \tilde{\iota}_{\hat{s}\hat{s}} + \tilde{\iota}_{qq}$. Next we find

$$u_{\pm 1} = 2\Omega\frac{3\Omega^2 + s^2}{\Omega_+}\tilde{\iota}_{\hat{s}\hat{s}} + 2\Omega\frac{s^2 - 3\Omega^2}{\Omega_+}\tilde{\iota}_{qq} \pm 12(\Omega^2 - s^2)\tilde{K}_{\hat{s}\hat{s}} \mp 6(\Omega^2 + 2s^2)\tilde{K}_{qq} \pm 24s^2\tilde{\Theta} - 12\Omega s\tilde{f}^{\hat{s}}, \tag{62}$$

propagating with speeds $\pm i\Omega$, which corresponds to light speed in the continuum system. At the continuum four characteristic variables in the scalar sector propagate at light speed. In the semidiscrete system with our discretization the third and fourth of these characteristics,

$$u_{\pm v_-} = \frac{3\bar{\mu}_S\Omega^2 - 3v_-^2 + s^2(\bar{\mu}_S - 1)}{6\Omega_+(v_-^2 - \Omega^2)} v_- \tilde{\Lambda} + \frac{3\bar{\mu}_S\Omega^2 - 3v_-^2 + s^2(\bar{\mu}_S - 1)}{\Omega_+(v_-^2 - \mu_L\Omega^2)} v_- \tilde{\epsilon} \pm \frac{s}{\Omega_+}\tilde{\phi}^{\hat{s}} \pm \frac{4s^2(\bar{\mu}_S - 1)}{(\mu_L - \bar{\mu}_S)(3v_-^2 - 4\Omega^2) - s^2\mu_L(\bar{\mu}_S - 1)}\bar{\mu}_S\tilde{\hat{K}} \pm 2\frac{3\bar{\mu}_S\Omega^2 - 3v_-^2 + \bar{\mu}_S s^2}{\Omega^2 - s^2}\tilde{\Theta} + \frac{\bar{\mu}_S - 1}{\Omega^2 - v_-^2} v_- s\tilde{f}^{\hat{s}}, \quad (63)$$

become coupled to the characteristic variables of the shift. They propagate with speeds $\pm v_-$, where we define $v_\pm$ by

$$v_\pm^2 = \tfrac{1}{6}(4 + 3\bar{\mu}_S)\Omega^2 + \tfrac{1}{6}(\bar{\mu}_S - 1)s^2 \pm \tfrac{1}{6}\sqrt{[(4 + 3\bar{\mu}_S)\Omega^2 + (\bar{\mu}_S - 1)s^2]^2 - 48\bar{\mu}_S\Omega^4}. \quad (64)$$

Under the substitution $\Omega \to s$ the continuum result (in Fourier space) is recovered. The last of the characteristic variables in the scalar sector are naturally associated with the gamma-driver condition. They are given by the same expression as (63) under the replacement $v_- \to v_+$, and have speeds $\pm v_+$. Special cases in the choice of the gauge parameters that prevent the existence of a complete set of characteristic variables in the scalar sector are discussed below. Thankfully in the vector sector we have the straightforward

$$u_{A\pm 1} = \frac{\Omega}{2\Omega_+}\tilde{\iota}_{\hat{s}A} \pm \tilde{K}_{\hat{s}A} - \frac{s}{2\Omega}\tilde{f}_A, \quad (65)$$

$$u_{A\pm\sqrt{\bar{\mu}_S}} = \frac{\Omega}{\Omega_+}\tilde{\phi}_A \pm \sqrt{\bar{\mu}_S}\tilde{f}_A, \quad (66)$$

with speeds $\pm i\Omega$ and $\pm\sqrt{\bar{\mu}_S}i\Omega$. Finally in the discretization of the gravitational wave degrees of freedom we have the trivial,

$$u^{\mathrm{TF}}_{AB\pm 1} = \frac{\Omega}{2\Omega_+}\tilde{\iota}^{\mathrm{TF}}_{AB} \pm \tilde{K}^{\mathrm{TF}}_{AB}, \quad (67)$$

with speeds $\pm i\Omega$, and where TF denotes that the trace is removed with respect to the projected background metric.

5. Special cases

Assuming that $\mu_L > 1$, there are two special cases in the choice of the gauge parameters μ_L, $\bar{\mu}_S$ under which the scalar sector does not admit the complete set of characteristic variables (61)–(63) given above. They are

$$[(4 + 3\bar{\mu}_S)\Omega^2 + (\bar{\mu}_S - 1)s^2]^2 - 48\bar{\mu}_S\Omega^4 = 0, \quad (68)$$

$$(3\mu_L - 4)(\mu_L - \bar{\mu}_S)\Omega^2 - \mu_L(\bar{\mu}_S - 1)s^2 = 0, \quad (69)$$

which correspond to $4\bar{\mu}_S = 3$ and $3\mu_L = 4\bar{\mu}_S$ at the continuum in curved space. These special cases are more subtle in the semidiscrete system because instability depends on both the background metric and the specific order of the discretization. Here we restrict our discussion to the trivial background metric δ_{ij}, the gauge parameter $\mu_L = 2$. Then for either $\bar{\mu}_S = \frac{3}{4}$ or $\bar{\mu}_S = \frac{3}{2}$, in the limit of high resolution, $h \to 0$, the characteristic variables become degenerate in a neighborhood of the grid mode $\xi_i = 0$. This situation is the same as that of the ADM formulation discussed in [38]. Any other mode satisfying (68) and (69) will be unstable. There are no such modes for $\mu_S < \frac{3}{4}$ or $\frac{3}{4} < \mu_S < \frac{3}{2}$ because for the standard second and fourth order discretizations $a = 1$ in (60) above with the Minkowski background. In the limit of high resolution, one also expects to find unstable modes in the region $\frac{3}{2} < \mu_S < 2$, although for particular choices of μ_S they may also appear at low resolutions. The general case is sketched in Fig. 1.

6. Numerical stability

Notice that at the lowest and highest grid frequencies the principal symbol takes a different form, because either Ω_+

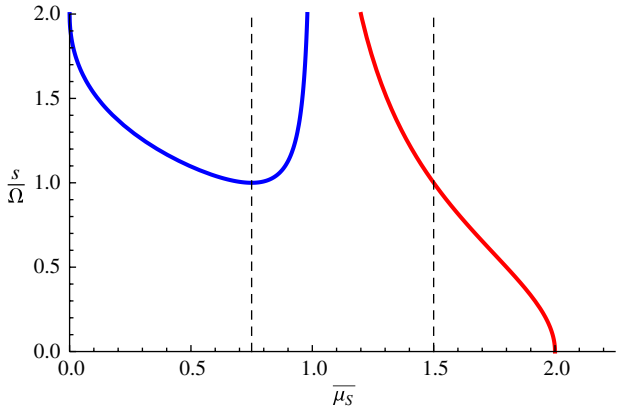

FIG. 1 (color online). The unstable gridmodes with the novel discretization and $\mu_L = 2$. The left (blue) line denotes (68) and the right (red) (69). The dashed vertical lines depict the choices of $\bar{\mu}_S$ that render the system weakly hyperbolic at the continuum level. For those choices no stable discretization is possible. In practice for the weakly hyperbolic choices of $\bar{\mu}_S$, the characteristic variables become singular at high resolution, preventing the construction of a symmetrizer independent of h. In principle, one expects to be able to find a stable discretization for all other values of $\bar{\mu}_S$, but our novel discretization does not fulfill that requirement. The unstable modes should be truncated in the y axis at some finite $a \gtrsim 1$ determined by the discretization and background metric, and so large values of unstable s/Ω are not to be considered troublesome. On the other hand, behavior of the red line in the region $3\mu_L/4 < \bar{\mu}_S < \mu_L$ is undesirable, because we always expect to find modes in that region on the numerical grid. Note that for our standard choice, $\mu_S = 1$, the blue line diverges, provided that the determinant of the background metric $\delta \simeq 1$, implying that our standard choice is stable, at least in that approximation. There are never unstable modes when $\mu_L < \bar{\mu}_S$.

or s^i vanish. As discussed in [38], this poses no difficulty in the constant coefficient case, provided that the principal symbol remains diagonalizable for those frequencies, as the full solution may be written as a direct sum over the modes. The principal symbol vanishes at the lowest frequency and so is trivially diagonalizable. At the highest frequency, by construction, the principal symbol can be written as that of a system of decoupled wave equations, and so is also trivially diagonalizable. The argument given in [38] guarantees that the standard method of lines time integrators will not violate the reduction constraints. The existence of a complete set of characteristic variables for the system for every grid frequency guarantees the existence of a symmetrizer $\hat{H}(s_i)$, which in turn guarantees numerical stability, namely that the estimate,

$$\|u(t_n,\cdot)\|_{h,D_+} \leq K e^{\alpha t_n} \|u(0,\cdot)\|_{h,D_+}, \tag{70}$$

holds for sufficiently small h, where α, K are constants, independent of h, that are not to be confused with the lapse and extrinsic curvature, provided that the Courant factor λ, the ratio of the time step and the spatial resolution, is chosen sufficiently small. The Courant condition is $\lambda \leq \alpha_0/(2\sqrt{3\mu_L})$, in the flat space, second order accurate case with $\mu_S = 1$ and α_0 the stability radius of the time integrator. The norm $\|\cdot\|_{h,D_+}$ is given by

$$\begin{aligned}\|u(t,\cdot)\|^2_{h,D_+} = {} & \|\alpha\|^2_h + \sum_{i=1}^{3} \|\beta^i\|^2_h + \sum_{i,j=1}^{3} \|\gamma_{ij}\|^2_h + \|\Theta\|^2_h \\ & + \sum_{i=1}^{3} \|f^i\|^2_h + \sum_{i,j=1}^{3} \|K_{ij}\|^2_h + \sum_{i=1}^{3} \|D_{+i}\alpha\|^2_h \\ & + \sum_{i,j=1}^{3} \|D_{+i}\beta^j\|^2_h + \sum_{i,j,k=1}^{3} \|D_{+i}\gamma_{jk}\|^2_h.\end{aligned} \tag{71}$$

7. Discussion

The inclusion of a constant background shift is straightforward since it affects the characteristic speeds in a trivial way, and has no affect on the characteristic variables. Different choices of discretization of the shift advection derivatives were studied in detail in [39]. Setting the background lapse to unity was done only for convenience and does not affect the results qualitatively. In the linear constant coefficient regime, the conformal variables can be expressed as a linear combination of the NOR variables that we have used in our calculations. The transformation to conformal variables is *not* however just a change of variables, because the transformation introduces the algebraic constraints D and T. In the linear constant coefficient case, as discussed in [40], if an explicit polynomial time integrator is used then linearity of the system guarantees that the algebraic constraints will not be violated if they are initially satisfied. The time integrator can furthermore be modified by a constraint projection step, so that even if the initial data does violate the algebraic constraints then numerical stability of the algorithm is trivially recovered. In the variable coefficient and nonlinear cases, the constraint projection step is essential because error will otherwise violate the algebraic constraints, and as shown in Appendix A, when the algebraic constraints are violated the Z4c formulation is generically only weakly hyperbolic. It would be desirable to extend the results presented in this section to the variable coefficient case, rather than linearizing and freezing coefficients. The most powerful method for doing so would be to use a summation by parts finite-differencing scheme to conserve a semidiscrete energy. Unfortunately, such an approach does not work because, as shown in Appendix B, even at the continuum level no such energy exists.

IV. THE APPLES WITH APPLES TESTS

A. Numerical setup

For our numerical tests, we use the AMSS-NCKU code [45–47]. The code employs message passing interface parallelization for moving box mesh refinement and method of lines time integration. In physics applications, the code uses the moving puncture gauge with BSSNOK to evolve black-hole spacetimes. Here it is used in a much simpler context: each of the apples with apples tests employs just a single mesh, and periodic boundary conditions in space, which avoids implementing complicated conditions in 3D. Following [48,49] we set simulation domain $x \in [-0.5, 0.5]$. In contrast to the normal AMSS-NCKU setup, we use an unstaggered, or vertex centered, grid $x_n = -0.5 + ndx$, $n = 0, \ldots, 50\rho$. We take $dx = dy = dz = 1/(50\rho)$, $\rho = 1, 2, 4$, and so on. In the y and z directions, following [49], we use only five grid points. The Courant factor $\lambda = dt/dx$ is taken to be either 0.1, 0.25, or 0.5 according to the specific goal of each test. For spatial derivatives, we restrict exclusively to second order accurate finite differencing. For advection terms $\beta^i \partial_i$, we use the upwind scheme

$$D_i^{(\mathrm{up})} = \begin{cases} D_{+i} - \frac{1}{2} dx_i D_{+i} D_{+i} & \text{if } \beta^i > 0, \\ D_{-i} + \frac{1}{2} dx_i D_{-i} D_{-i} & \text{if } \beta^i < 0. \end{cases} \tag{72}$$

For the remaining spatial derivatives we employ either the standard spatial discretization (25), or the novel scheme described in Sec. III A. In [50] it was shown, albeit for gauge conditions other than those that we employ here, that without artificial dissipation the BSSNOK formulation is not numerically stable. Since we are comparing the Z4c formulation with BSSNOK, we therefore always use Kreiss-Oliger numerical dissipation [42],

$$\partial_t u \rightarrow \partial_t u - \sigma \sum_{i=1}^{3} dx_i^3 (D_{i+} D_{i-})^2 u, \tag{73}$$

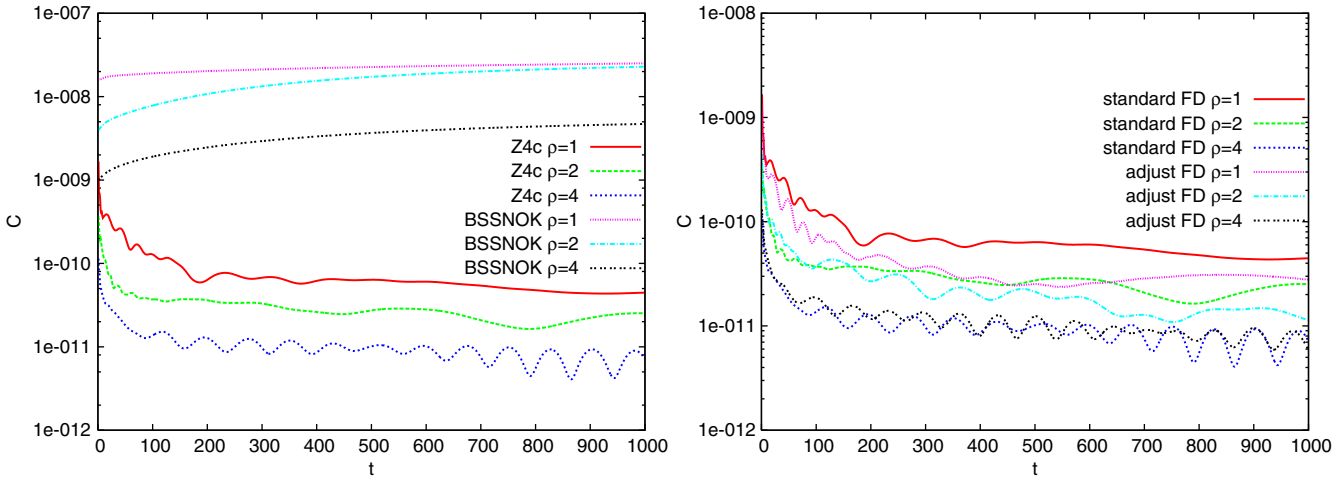

FIG. 2 (color online). Comparison of the constraint violation monitor (74) for the robust stability test with $\eta = 2$. The left subplot compares BSSNOK and Z4c, where the standard discretization scheme is used. Numerical experiments reveal that the drop in the constraint monitor in the Z4c tests is caused neither by artificial dissipation nor the η parameter. The right subplot compares the standard discretization scheme and the novel discretization scheme for Z4c formalism.

with dissipation parameter $\sigma = 0.02$. In the original apples with apples tests, gauge conditions were prescribed. Unfortunately some of those prescriptions result in an ill-posed initial value problem when coupled to either the BSSNOK or Z4c formulations. Furthermore, we prefer to study error properties of the exact system that we will later use to perform astrophysical simulations. We therefore use only the puncture gauge (22) and (23) with $\mu_L = 2/\alpha$, $\mu_S = 1/\alpha^2$, and $\eta = 2$ unless stated otherwise. We are mainly concerned with the effect of each formulation on the accuracy of the numerical calculation at finite resolution and the effect of the novel discretization scheme versus the standard discretization for the Z4c system. In our tests we frequently use the constraint monitor

$$C \equiv \begin{cases} \sqrt{H^2 + \gamma_{ij} M^i M^j + \Theta^2 + 4\gamma_{ij} Z^i Z^j} & \text{for Z4c,} \\ \sqrt{H^2 + \gamma_{ij} M^i M^j + \gamma_{ij} G^i G^j} & \text{for BSSNOK} \end{cases} \tag{74}$$

to assess the quality of the numerical solution. Here H is the Hamiltonian constraint violation, M^i is the momentum constraint violation, and G^i is the Gamma constraint violation. Since $2Z^i$ corresponds to the Gamma constraint in BSSNOK formalism, we use $4\gamma_{ij} Z^i Z^j$ to mimic the Gamma constraint violation part.

B. Robust stability test

First we perform the robust stability test. Besides the gauge choice we follow the original prescription. Initially all variables including lapse and shift are set to the Minkowski value perturbed by a random number $\epsilon \in (-10^{-10}/\rho^2, 10^{-10}/\rho^2)$. We set the Courant factor to $\lambda = 0.5$. In Fig. 2, the constraint violation monitor with respect to time is plotted for evolutions with $\eta = 2$. In the left subplot we compare Z4c formalism with BSSNOK formalism using in each case the standard discretization scheme. Although neither BSSNOK nor Z4c suffer from rapid undesirable growth of the solution, the constraint violations are slowly increasing for BSSNOK formalism while they are decreasing in the Z4c test. By the end of the evolution, the constraint violations in the Z4c tests are several orders of magnitude lower than those of the BSSNOK test. We do not have an explanation for this behavior. The usual argument is that the propagating constraint subsystem of the Z4c formulation should prevent constraint violation from growing on the grid, but in this test the constraint violation cannot be absorbed by the boundary conditions. To investigate the cause of the decay of the constraints we have performed tests without artificial dissipation. There we find that the constraint violation levels off around an order of magnitude above the value obtained with artificial dissipation. We also tried evolutions with $\eta = 0$, and find that the constraint monitor is larger than with $\eta = 2$, but that the qualitative behavior is unaltered. Experimenting with the constraint damping scheme with $\kappa_1 = 0.02$, $\kappa_2 = 0$, we find a minor improvement in the constraint monitor, in line with our expectation from the results of [34]. In the right subplot, we compare the standard discretization scheme and the novel scheme, for which we have a proof of numerical stability in the constant coefficient approximation, each with the Z4c formalism. Here, however, we would like to reiterate the important point made in [38], namely that formal numerical stability neither implies nor is implied by robust stability. The robust stability test, in the form studied here, should be viewed only as a gauge of the errors present in the numerical evolution at a finite resolution. In

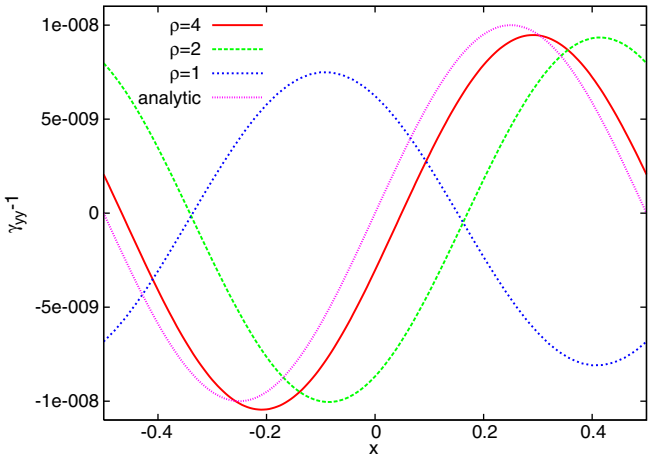

FIG. 3 (color online). Snapshots of $\gamma_{yy} - 1$ at coordinate $t = 1000$ for Z4c formalism at different resolutions with the standard discretization scheme and initial data corresponding to a linearized gravitational wave. The evolution is performed with the puncture gauge. The phase of the wave appears to be converging to the linear analytic solution.

Appendix A we present more demanding convergence tests.

C. Linear wave test

The second test is the evolution of a linearized gravitational wave on the Minkowski background. We set initial data as

$$\begin{aligned} &\gamma_{xx} = 1, \qquad \gamma_{yy} = 1 + b, \qquad \gamma_{zz} = 1 - b, \\ &\alpha = 1, \qquad K_{yy} = \tfrac{1}{2}\partial_t b, \qquad K_{zz} = -\tfrac{1}{2}\partial_t b, \end{aligned} \tag{75}$$

and the remaining variables to zero. Here we choose

$$b = A \sin\left[\frac{2\pi(x-t)}{d}\right], \tag{76}$$

and $d = 1$, $A = 10^{-8}$. The Courant factor is chosen $\lambda = 0.5$. Such a small perturbation of the metric ensures that the numerical evolution remains essentially in the linear regime. Here the initial data are constraint violating, and the puncture gauge condition is not necessarily compatible with simple advection of the wave profile. In practice, however, it appears that to a good approximation the solution is a simple traveling wave; in Fig. 3 we compare the final γ_{yy} numerical profile, obtained with Z4c, to the analytic solution of the linearized Einstein equations with unit lapse and zero shift. There it appears that at least the phase of the numerical solution is converging with resolution to the analytic solution. A more meaningful evaluation of the errors in the system is obtained by performing self-convergence tests on the data, for which we use the D_+ norm (71) evaluated on the conformal variables of the Z4c and BSSNOK formulations. There we find perfect second order convergence in the norms for both BSSNOK and Z4c (Fig. 4, BSSNOK gives the same behavior as Z4c, not shown), and estimate that after 1000 light-crossing times, the error is approximately 2×10^{-9} for resolution $\rho = 4$ and 8 (Fig. 4). Since the initial data for these evolutions is constraint violating we do not present the constraint monitor for this test, although we find that here it stays around 1×10^{-12} with either formulation. The novel discretization for Z4c gives almost identical results to those of the standard discretization. We tested the effect of constraint damping terms and different values of η in the gamma-driver shift. Neither has an effect on the result of these tests. Concerning coordinate gauge conditions, for comparison, we have performed additional evolutions with harmonic lapse, $\mu_L = 1$ in (22) with harmonic shift (24). We find both choices give very similar same convergence behavior and errors.

In addition to the above sine wave test, we also adopted the Gaussian shaped linear wave test suggested in [51]. Instead of Eq. (76), the b takes

$$b = A \exp\left[-\frac{(x-t)^2}{2w^2}\right], \tag{77}$$

with $A = 10^{-8}$. In order to get periodic profile initially we set $w = 0.5$ which makes b roughly 0 at $x = \pm 0.5$. Since the effective wavelength for this Gaussian wave is 1 which is one-tenth of the wavelength of above sine wave, we need more resolution to get reasonably convergent results. Reducing numerical dispersion requires more resolution still. In all we find resolutions $\rho = 16$, 32, and 64 can produce good convergence results (Fig. 5). The error for $\rho = 64$ and 32 is comparable to the $\rho = 8$ and 4 of sine wave case, which is roughly 2×10^{-9}.

As to the two-dimensional sine wave test,

$$\begin{aligned} &\gamma_{xx} = \gamma_{yy} = 1 + \frac{H}{2}, \qquad \gamma_{xy} = \frac{H}{2}, \qquad \gamma_{zz} = 1 - H, \\ &K_{xx} = K_{yy} = K_{xy} = \frac{1}{4}\partial_t H, \qquad K_{zz} = -\frac{1}{2}\partial_t H, \\ &H = A \sin\left[\frac{2\pi(x - y - \sqrt{2}t)}{d}\right], \qquad \alpha = 1, \end{aligned} \tag{78}$$

$d = 1$, $A = 10^{-8}$ and other variables zero, the result is similar to the one-dimensional test. But because the effective wavelength for two-dimensional sine wave is $1/\sqrt{2}$, a little higher resolution ($\rho = 2, 4, 8$) is needed to get comparable convergence behavior as in the one-dimensional case (Fig. 6). As in the earlier robust stability tests the constraint damping scheme with $\kappa_1 = 0.02$, $\kappa_2 = 0$ reduces the constraint violation very little.

D. Gauge wave and shifted gauge wave tests

The third and fourth tests are the unshifted gauge wave and shifted gauge wave tests. For the gauge wave test we take

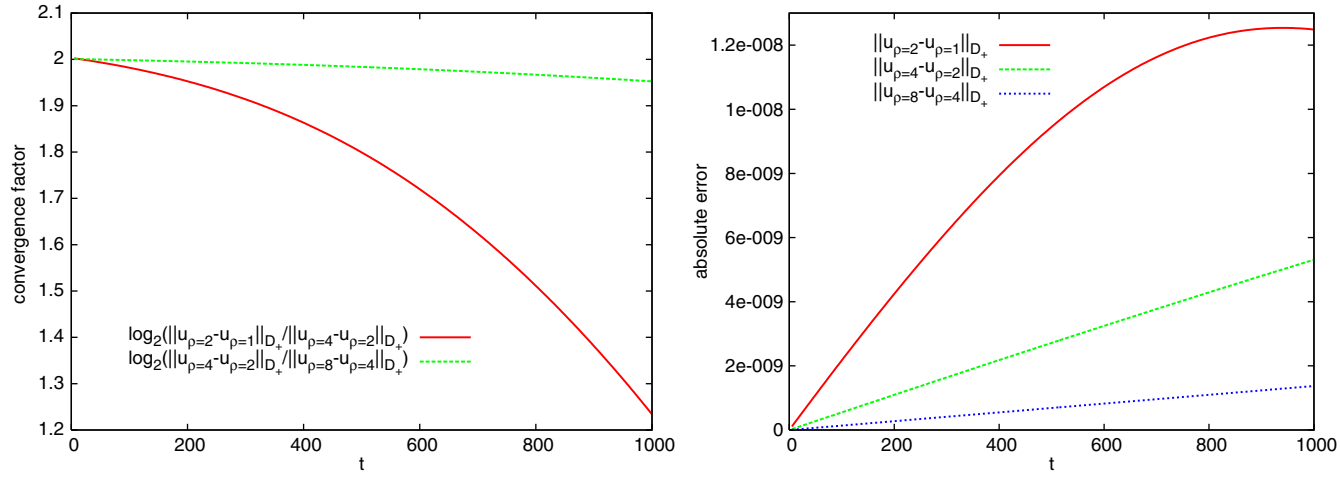

FIG. 4 (color online). Here we plot the experimental convergence factor (left panel) and an approximation of the absolute error (right panel) for the "x" direction sine linear wave test with amplitude $A = 10^{-8}$. The evolution was performed with the puncture gauge and the standard discretization. So that two self-convergence tests could be presented grids with $\rho = 1, 2, 4, 8$ were used. As expected, the self-convergence test at higher resolution results in an experimental convergence factor closer to 2 for longer.

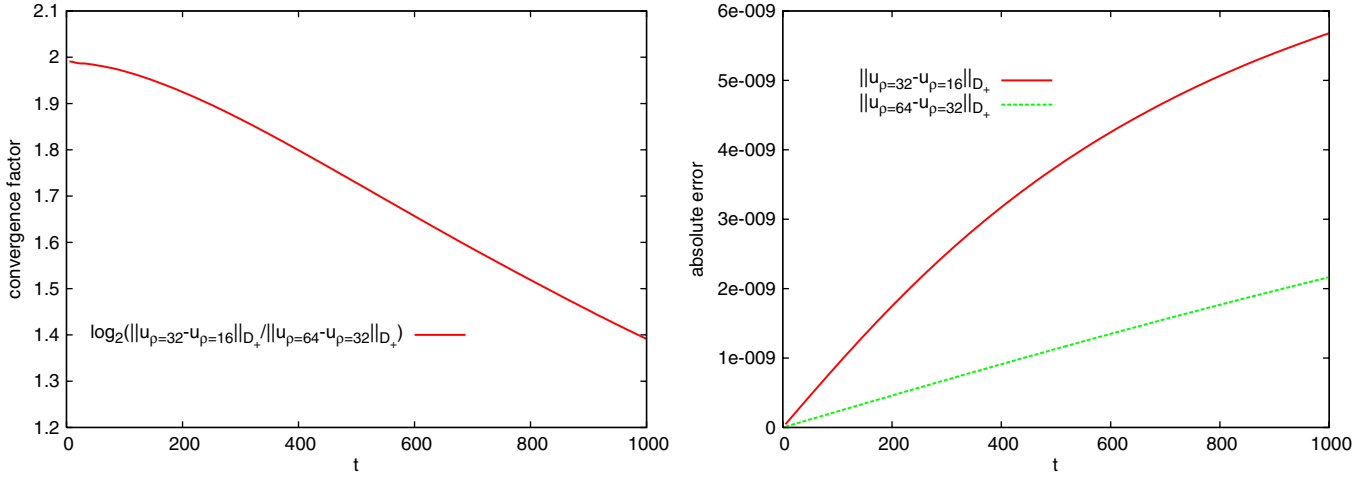

FIG. 5 (color online). Here we plot the experimental convergence factor (left panel) and an approximation of the absolute error (right panel) for the "x" direction Gaussian profile linear gravitational wave test with amplitude $A = 10^{-8}$. As in Fig. 4, the evolution was performed with the puncture gauge and the standard discretization. In contrast to the tests presented in Fig. 4, here a higher resolution, $\rho = 16, 32, 64$, was used so that the Gaussian profile could be resolved.

$$\gamma_{xx} = 1 - b, \qquad \gamma_{yy} = 1, \qquad \gamma_{zz} = 1,$$
$$K_{xx} = \frac{\partial_t b}{2\sqrt{1-b}}, \qquad \alpha = \sqrt{1-b}, \tag{79}$$

as initial data. For the shifted gauge wave we use

$$\gamma_{xx} = 1 + b, \qquad \gamma_{yy} = 1, \qquad \gamma_{zz} = 1,$$
$$K_{xx} = \frac{\partial_t b}{2\sqrt{1+b}}, \qquad \alpha = \frac{1}{\sqrt{1+b}}, \qquad \beta^x = -\frac{b}{1+b}, \tag{80}$$

and in either case set the remaining variables to zero. We again choose (76), but now with $d = 1$. Both $A = 0.01$ and $A = 0.1$ are tested. We set the Courant factor $\lambda = 0.5$ in the unshifted case and $\lambda = 0.25$ in the evolution with nontrivial initial shift. Otherwise the grid setup is the same as in the robust stability test. It is well known that with harmonic lapse, $\mu_L = 1$, and vanishing shift the BSSNOK formulation suffers from large undesirable growth of the errors in both of these tests [49]. We recover that behavior with BSSNOK, and find that with the Z4c system the blowup is delayed. The growth can be anticipated from the results of [10,52,53], which show that the harmonic gauge admits exponential growth in time evolution of such initial data. For a direct comparison with the gauge wave results of [35] we performed this test with harmonic lapse, vanishing shift and constraint damping and $\kappa_1 = 1$, $\kappa_2 = 0$. There, in agreement with [35] we

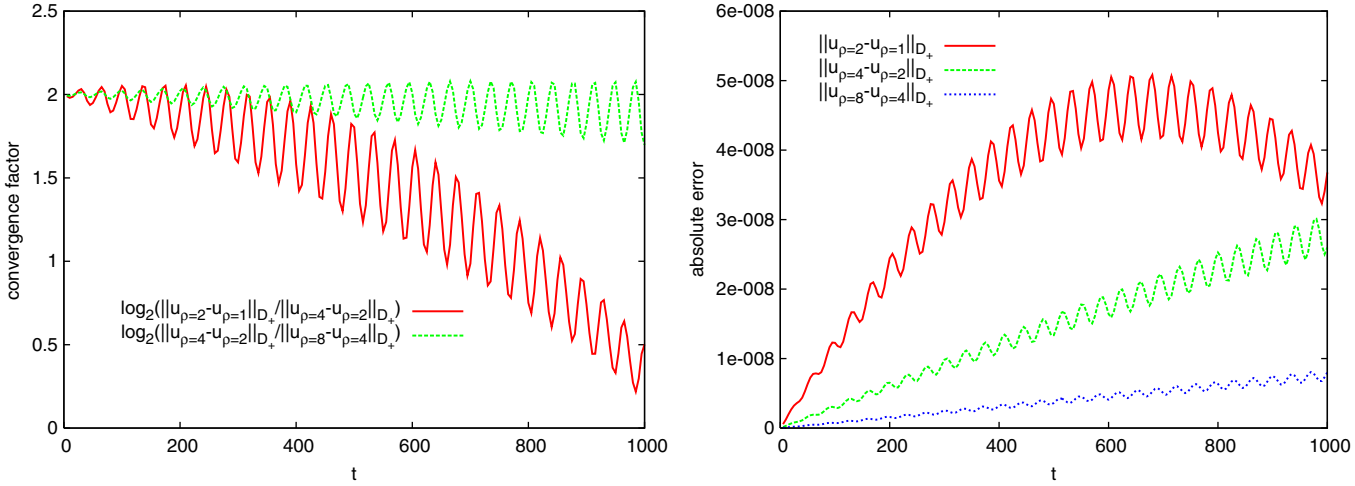

FIG. 6 (color online). The plot is identical to Fig. 4 except that here the diagonal sine wave (81) was evolved. The errors are correspondingly larger than in the one-dimensional test, but still we find that at higher resolution the experimental convergence factor stays close to 2 for longer.

find that the errors do not result in a code crash, although at this resolution the experimental convergence factor is very poor. In contrast to the harmonic lapse gauge condition, the puncture gauge is able to evolve the gauge wave for 1000 light-crossing times with no sign of blowup without constraint damping. It would be interesting to know what concrete feature of the puncture gauge suppresses the growth admitted by the harmonic gauge. Since both $A = 0.01$ and $A = 0.1$ give roughly the same result, in Fig. 7 we plot the convergence factor and the D_+ norm of the error only for $A = 0.01$. As the first test of nonlinear effects in "apples with apples" test suite, Z4c gives better convergence behavior than BSSNOK. As shown in the left subplot of Fig. 7, Z4c can approximately maintain a convergence factor around two while BSSNOK drops to negative values. Moreover, Z4c gives more than one order smaller error as shown in the right subplot of Fig. 7. In terms of constraint violation we find that without Z4c constraint damping the constraint monitor is comparable for the two formulations throughout the evolutions. On the other hand, we find that with $\kappa_1 = 0.02$, $\kappa_2 = 0.0$, the Z4c constraint violation is an order of magnitude smaller than that of BSSNOK at the end of the evolution. The experimental convergence factor is unaffected by the use of the constraint damping scheme in this test. Furthermore, we find that with the puncture gauge condition the coordinates are rapidly driven to match inertial coordinates of Minkowski space. In others words, the amplitude of the

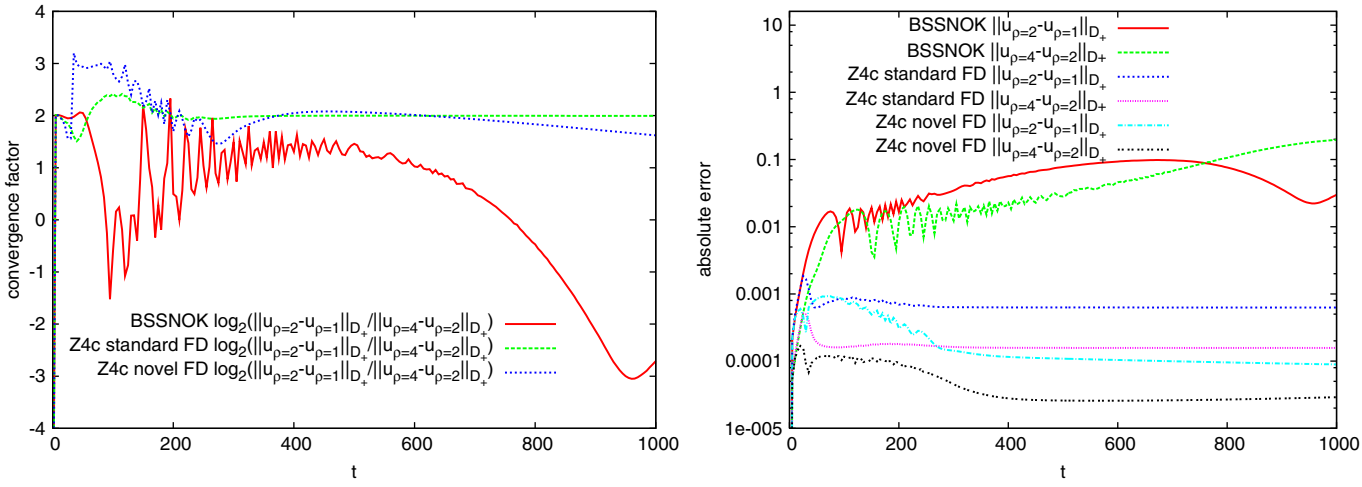

FIG. 7 (color online). In this plot we present the experimental convergence factor (left panel) and an approximation of the absolute error (right panel), obtained with the puncture gauge for BSSNOK and Z4c with the standard discretization and Z4c with the novel discretization, obtained in the evolution of the one-dimensional gauge wave initial data (79) of amplitude $A = 0.01$ with the puncture gauge. The Z4c tests seem to maintain near second order convergence for longer, and the errors in the BSSNOK evolution are roughly an order of magnitude greater than those of Z4c over the evolution.

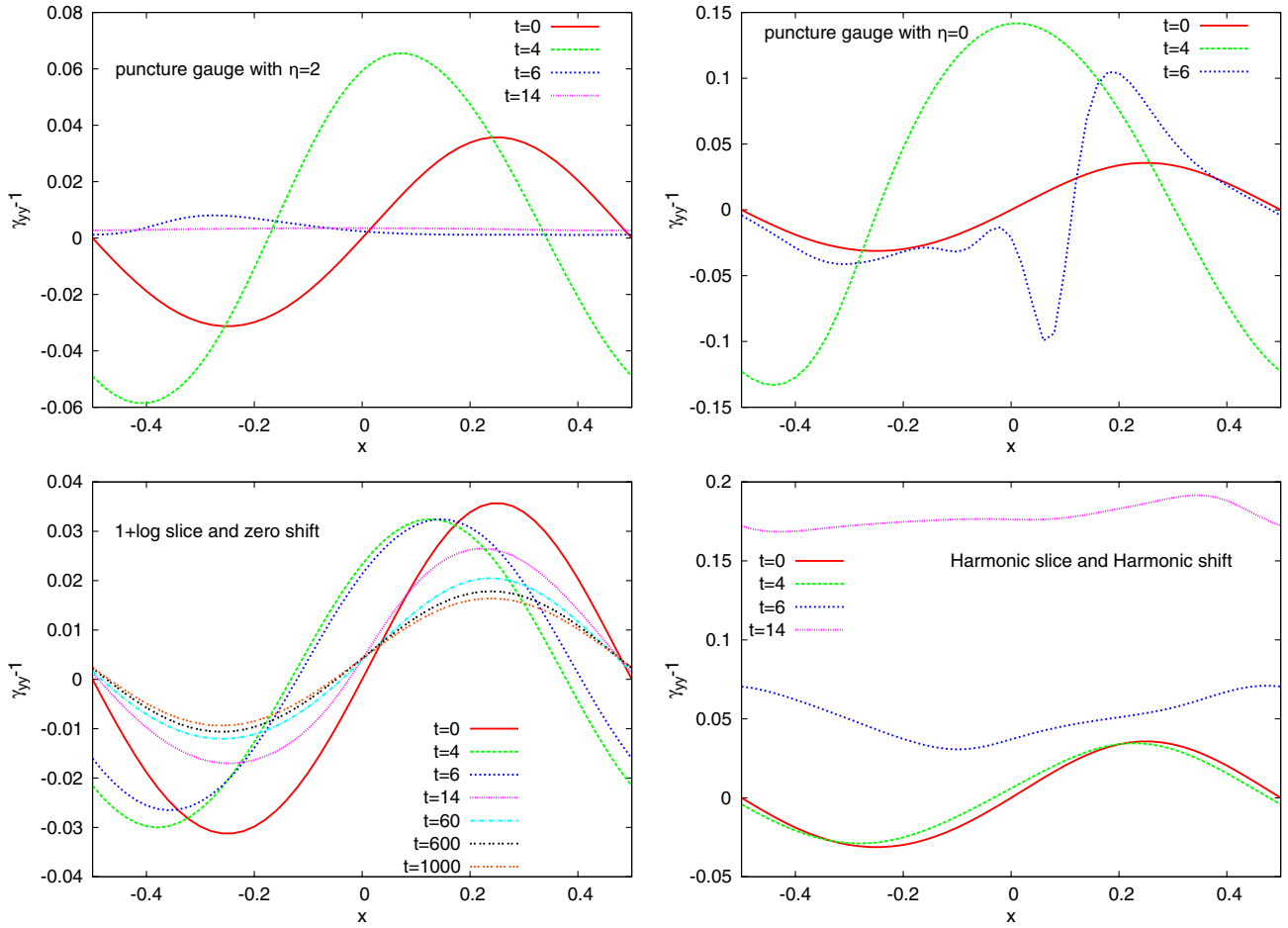

FIG. 8 (color online). Gauge wave test with the puncture gauge condition [(22) and (23), $\eta = 2$ or 0], with 1 + log slice and zero shift and with harmonic lapse and harmonic shift. Here $\gamma_{yy} - 1$ is plotted at coordinate times 0, 2, 6, and 14, respectively, for a test performed with the Z4c formalism and the standard discretization scheme. With puncture gauge and $\eta = 2$, the gauge wave is rapidly suppressed by the gauge condition and at later times $\gamma_{yy} - 1$ tends to zero. While with other gauge conditions we cannot see this symmetry seeking property; with $\eta = 0$ the code crashes soon after $t = 7.2$.

gauge wave decreases, as shown in Fig. 8, so in some sense, the puncture gauge condition possesses a symmetry seeking property. As shown in this figure, we find that other gauge conditions do not have this property and the nonzero value of η is also essential for the successful evolution. Note that this gauge condition is similar to that used in binary black-hole simulations. The novel discretization gives near identical results to the standard discretization. Tests with the harmonic gauge result in both larger absolute error and larger constraint violations.

As for the two-dimensional linear wave test, we use

$$\gamma_{xx} = \gamma_{yy} = 1 - \frac{H}{2}, \qquad \gamma_{xy} = \frac{H}{2}, \qquad \gamma_{zz} = 1,$$
$$K_{xx} = K_{yy} = -K_{xy} = \frac{\partial_t H}{4\sqrt{1-H}}, \qquad K_{zz} = -\frac{1}{2}\partial_t H, \qquad (81)$$
$$H = A \sin\left[\frac{2\pi(x - y - \sqrt{2}t)}{d}\right], \qquad \alpha = \sqrt{1-H},$$

with $d = 1$, $A = 0.01$, 0.1 for initial data for the two dimensional gauge wave test, which corresponds to the wave propagating along the diagonal direction of x-y plane. The results are similar to the one-dimensional tests.

As for the shifted gauge wave test, the original "apples with apples" test suggested $A = 0.5$. We find such a large amplitude results in code crashes for both formalisms with any coordinate gauge under consideration. Our findings are similar to those found with a pseudospectral method as used in the SPEC code [51]. The unshifted gauge wave tests also fail with amplitude $A = 0.5$. Restricting to $A = 0.1$, 0.01, we find the resulting error and the convergence behavior is very similar to the unshifted case. As an example we compare the two results with $A = 0.01$ in Fig. 9.

E. Gowdy wave test

The final tests are the expanding and collapsing Gowdy waves. Following the suggestion of [48,49], we choose for initial data

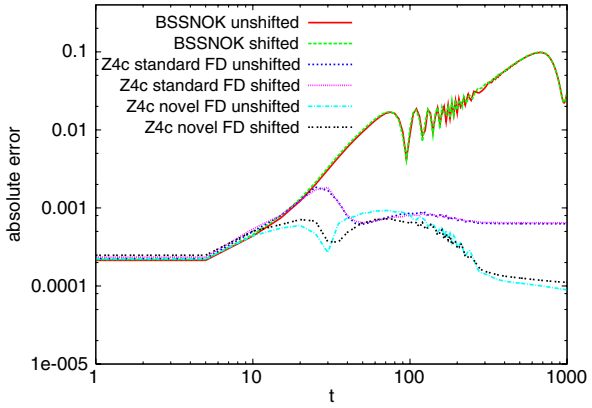

FIG. 9 (color online). In this plot we compare the D_+ norm of the error $\|u_{\rho=2} - u_{\rho=1}\|_{D_+}$ of the unshifted gauge wave test and the shifted gauge wave test. The evolutions were performed with the puncture gauge.

$$
\begin{aligned}
\gamma_{xx} &= t^{-1/2} e^{\Lambda/2}, \\
\gamma_{yy} &= t e^{P}, \\
\gamma_{zz} &= t e^{-P}, \\
K_{xx} &= \pm\tfrac{1}{4} t^{-1/4} e^{\Lambda/4} (t^{-1} - \Lambda_{,t}), \\
\alpha &= t^{-1/4} e^{\Lambda/4}, \\
K_{yy} &= \pm\tfrac{1}{2} t^{1/4} e^{-\Lambda/4} e^{P} (-1 - t P_{,t}), \\
K_{zz} &= \pm\tfrac{1}{2} t^{1/4} e^{-\Lambda/4} e^{-P} (-1 + t P_{,t}),
\end{aligned}
\tag{82}
$$

where the + sign is for the expanding Gowdy wave test and the − sign is for the collapsing Gowdy wave test, and other variables zero. Here $P = J_0(2\pi t)\cos(2\pi x)$ and

$$
\begin{aligned}
\Lambda = & -2\pi t J_0(2\pi t) J_1(2\pi t) \cos^2(2\pi x) \\
& + 2\pi^2 t^2 [J_0^2(2\pi t) + J_1^2(2\pi t)] \\
& - \tfrac{1}{2}[(2\pi)^2 [J_0^2(2\pi) + J_1^2(2\pi)] \\
& - 2\pi J_0(2\pi) J_1(2\pi)],
\end{aligned}
\tag{83}
$$

where J_n are Bessel functions. Initially we set $t = 9.875\,320\,582\,909\,8$ following [48,49] exactly. The Courant factor is set as $C = 0.05$. Here the use of the puncture gauge is troublesome because it does not reproduce the preferred analytical gauge in the evolution. Unfortunately, simply choosing the lapse and shift *a priori* results in an ill-posed initial value problem, highlighting the fact that in numerical relativity there are still open questions related to the choice of gauge conditions. Obviously conditions must be chosen that render the initial value problem well posed, but on the other hand such conditions may not correspond to those best suited to study a problem analytically.

The test results of expanding Gowdy wave are plotted in Fig. 10. Although this test is very tough [49], up to 1000, neither the BSSNOK formalism nor the Z4c formalism suffer from large growth of the errors causing the code to crash. Our results demonstrate the robustness of puncture gauge condition. In the left subplot, we show the behavior of relative error for two different resolutions where $\rho = 2$ and $\rho = 4$ are used. From this result we can see the increasing behavior of the error roughly follows the power function of t instead of the exponentially increasing result obtained by the spectral code in [51]. In the right subplot we show the constraint monitor with respect to time. In Fig. 11 we compare the convergence behavior with respect to Hamiltonian constraint violation. We find that Z4c

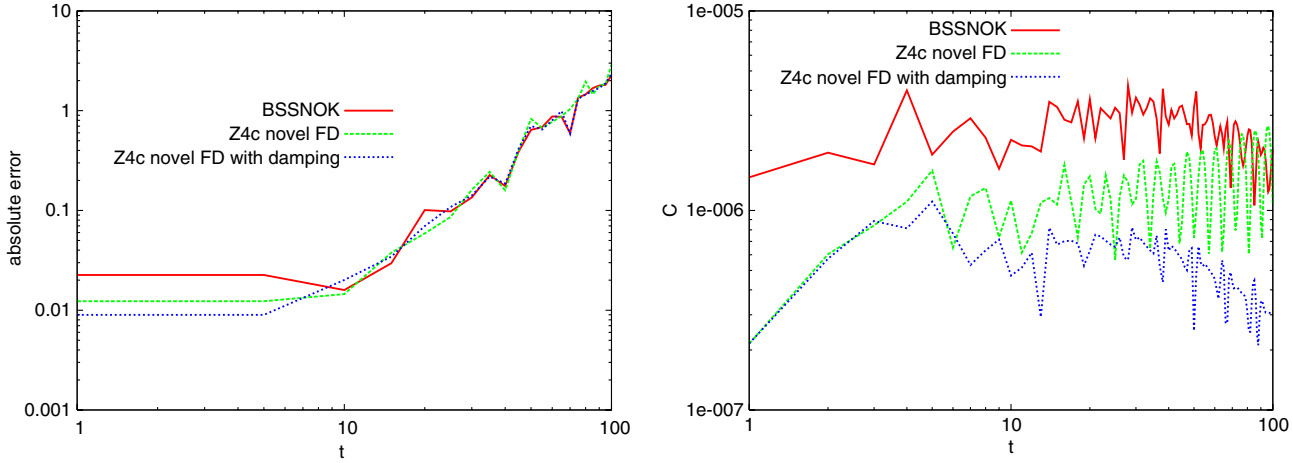

FIG. 10 (color online). Expanding Gowdy wave test with the puncture gauge condition. Courant factor $C = 0.05$ is used. The left panel shows the D_+ norm of the difference between the solutions with resolutions $\rho = 4$ and $\rho = 2$. The right subplot compares the constraint monitor with respect to time for BSSNOK formalism and Z4c formalism. For Z4c formalism we only show the novel finite difference scheme here because the standard finite difference scheme gives almost the same result. Here for Z4c formalism, with ($\kappa_1 = 0.02$, $\kappa_2 = 0$) and without damping terms are also compared. The constraint damping scheme does seem to be effective in this scenario, but has little effect on the absolute error.

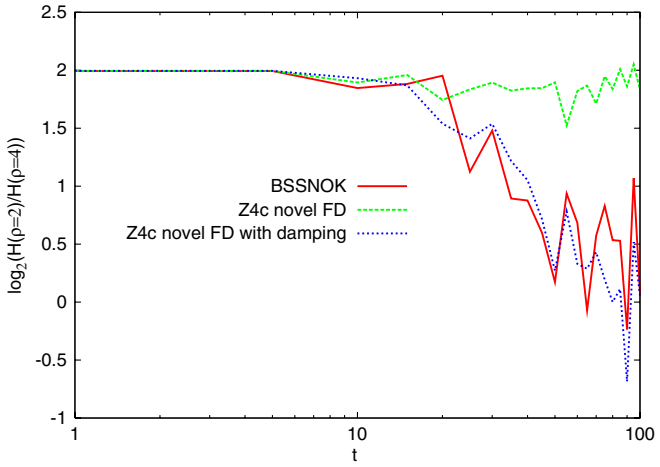

FIG. 11 (color online). Here we plot the experimental convergence factor for the Hamiltonian constraint in the expanding Gowdy wave test with the puncture gauge condition. Courant factor $C = 0.05$ is used. Since we have a trivial exact solution, the factor is computed using just the data from the higher resolution runs, $\rho = 2, 4$. The factor is $\log_2(\frac{H(\rho=2)}{H(\rho=4)})$, where $H(\rho)$ means the Hamiltonian constraint violation for resolution ρ. The constraint damping scheme does not appear to help in convergence of the constraints in this test.

formalism achieves better convergence results than BSSNOK formalism at this resolution. Once again the novel finite difference scheme gives almost exactly the same result as the standard discretization. If the damping term with $\kappa_1 = 0.02$ and $\kappa_2 = 0$ is used, the constraint violation is significantly reduced, but, as shown in Fig. 10, does not reduce the D_+ norm of the difference between two resolutions. Unfortunately, in Fig. 11 we see that the damping term does reduce the experimental convergence factor.

For the collapsing Gowdy wave, in contrast to the proposal of original "apples with apples" tests, we do not transform the time coordinate to avoid singularity by hand. Instead we simply change the sign of initial extrinsic curvature K_{ij} in Eq. (82) and evolve with the puncture gauge. Until 1000 light-crossing times, when we stop the test, the code does not crash. As the solution approaches the singularity, the puncture gauge makes the evolution effectively stop by the collapse of the lapse. Both BSSNOK and Z4c formalism gives almost identical results. In Fig. 12 we show several snapshots for the lapse and shift vector, and the singularity avoiding property of puncture gauge condition can be clearly seen. Since BSSNOK and Z4c formalisms give similar results, only BSSNOK results are shown. For the collapsing Gowdy test we find that the effect of the constraint damping scheme, with $\kappa_1 = 0.02$, $\kappa_2 = 0$, is negligible.

V. CONCLUSIONS

In order to demonstrate that a conformal decomposition of the Z4 formulation of general relativity may be a useful tool for numerical relativity simulations in three spatial dimensions, we have studied numerical stability of the system coupled to the moving puncture gauge condition. First, we proved that in combination with a novel discretization scheme, and periodic boundary conditions in space, the Z4c system is numerically stable when linearized around a constant background metric. We would like to extend our results to the variable coefficient case, but since Z4 coupled to the puncture gauge appears to be only strongly, but not symmetric hyperbolic, see Appendix B, there are few methods to hand. We then performed a complete set of the "apples with apples" tests, which we modified slightly to take into account the status of the

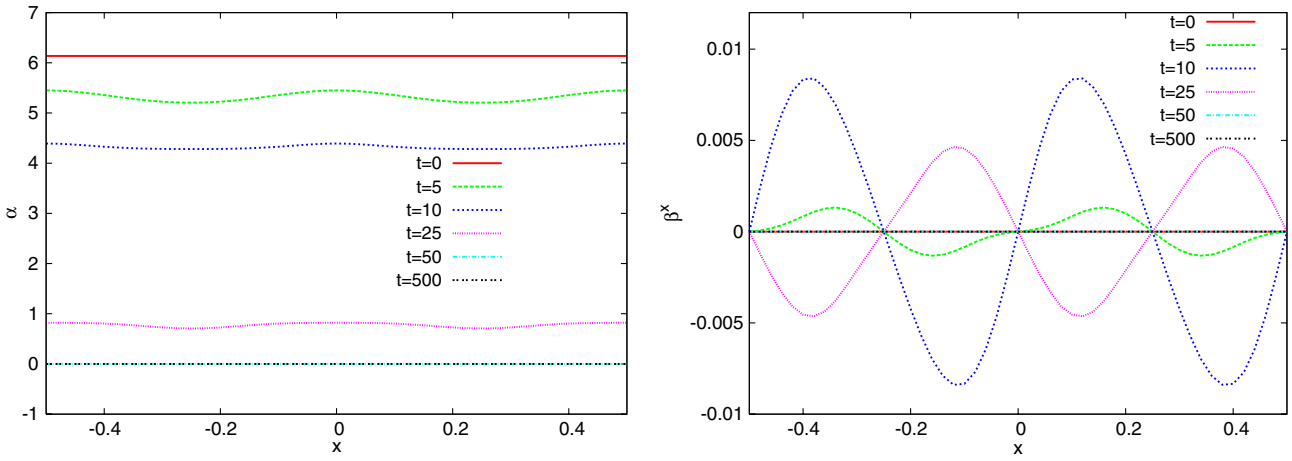

FIG. 12 (color online). Snapshots from the collapsing Gowdy wave test with Courant factor 0.05. BSSNOK formalism is used with resolution $\rho = 1$. The left subplot shows the snapshot of α at different coordinate times. The right subplot is β^x. α approaches 0 to freeze the evolution. β^x increases at very early time to adapt the evolution and decreases to 0 also soon afterwards. The puncture gauge makes the evolution freeze, at a proper time $\Delta\tau \simeq 8.7$ for the observer at the origin, before intersecting the singularity.

initial value problem from the PDEs point of view, and discussed for each the relative behavior of Z4c in comparison with BSSNOK. We summarize the results of the tests as follows.

A. Robust stability

In the robust stability tests we found that the Z4c evolutions result in a smaller constraint violation, a feature that was insensitive to the choice of gauge.

B. Linear waves

In the linear wave test we found only marginal differences between the two formulations, regardless of gauge conditions. It is perhaps expected that in this test the differences will be small, because the propagation of gravitational waves is of course a feature shared by both systems.

C. Gauge waves

For the gauge waves test we found, using the puncture gauge, that the Z4c evolutions exhibit an experimentally computed self-convergence factor closer to the expected second order than the BSSNOK data over many light-crossing times. In this context we found that the puncture gauge has a strong symmetry seeking effect and rapidly pushes the lapse to a constant, and the shift to zero.

D. Gowdy waves

To evolve expanding and collapsing Gowdy spacetimes we again employed the puncture gauge. Here we find that, although neither Z4c or BSSNOK results in code crashes, long-term convergence is very difficult to achieve. Another problematic feature here is that, although the puncture gauge results in a well-posed initial value problem for each of the formulations, it does not track the preferred coordinates on the spacetime under consideration.

In Appendix A we also studied the effect of the algebraic constraint projection on numerical convergence. When the algebraic constraints are violated, the Z4c formulation is only weakly hyperbolic, which is reflected in numerical approximation as a failure to converge to the continuum solution, even for trivial initial data such as noise on top of the Minkowski spacetime.

The evidence for the usefulness of a conformal decomposition of the Z4 formulation in astrophysical applications is mounting. In spherical symmetry, the system was shown to have favorable properties over BSSNOK [25], especially in the evolution of spacetimes containing matter. The trivial wavelike nature of the constraint subsystem was then used to construct high-order constraint preserving boundary conditions [33], which were studied in numerical applications in spherical symmetry. The constraint damping scheme for the formulation was studied in detail in [34]. There, once again in spherical symmetry, the efficacy of the constraint damping scheme was studied in numerical applications and it was found that the constraint damping scheme is a useful tool for the suppression of violations in vacuum spacetimes, but that when matter is present more work is required to paint a clear picture. For the first time, numerical evolutions of binary black-hole spacetimes with a conformal decomposition of Z4, CCZ4 were presented in [35]. Here we have focused on formal numerical stability, and compared numerical results obtained with BSSNOK and Z4c in a simple context. Overall we find some benefit to the use of Z4c, although in some sense the tests we have performed here, namely the evolution of vacuum spacetimes with periodic boundary conditions, are not optimally suited to the advantages found in spherical symmetry. In our view two points remain to be addressed before one can consider a wholesale replacement of BSSNOK in applications. First, it is desirable to obtain boundary conditions that are constraint preserving, minimize the incoming gravitational wave content, lead to a well-posed initial boundary value problem, and can be implemented in a 3D production code. Second, conclusive evidence of the benefits of Z4c over BSSNOK is needed in applications. We hope to address both of these issues shortly.

ACKNOWLEDGMENTS

The authors would like to thank Dana Alic, Sebastiano Bernuzzi, Carles Bona, Bernd Brügmann, Carsten Gundlach, Ian Hinder, Sascha Husa, Carlos Palenzuela, Vasileios Paschalidis, Luciano Rezzolla, Milton Ruiz, Yuichiro Sekiguchi, and Andreas Weyhausen for helpful discussions and/or comments on the manuscript. This work was supported in part by DFG Grant No. SFB/Transregio 7 "Gravitational Wave Astronomy" and by the NSFC (No. 11005149).

APPENDIX A: Z4C WITHOUT ENFORCEMENT OF THE ALGEBRAIC CONSTRAINTS

1. Weak hyperbolicity with the puncture gauge

Without assuming that the algebraic constraints are enforced, the equations of motion for the Z4c formulation cannot naturally be written in terms of the ADM variables. Under the standard 2 + 1 decomposition [54] and up to transverse and nonprincipal derivatives, they are given by

$$\partial_t \chi = \tfrac{2}{3}\chi[\alpha(\hat{K} + 2\Theta) - \partial_s \beta^s] + \beta^s \partial_s \chi, \tag{A1}$$

$$\partial_t \tilde{\gamma}_{ss} = -2\alpha \tilde{A}_{ss} + \tfrac{4}{3}\chi \partial_s \beta^s + \beta^s \partial_s \tilde{\gamma}_{ss}, \tag{A2}$$

$$\partial_t \tilde{\gamma}_{qq} = -2\alpha \tilde{A}_{qq} - \tfrac{4}{3}\chi \partial_s \beta^s + \beta^s \partial_s \tilde{\gamma}_{qq}, \tag{A3}$$

$$\partial_t \alpha = -\mu_L \alpha^2 \hat{K} + \beta^s \partial_s \alpha, \tag{A4}$$

$$\partial_t \beta^s = \alpha^2 \mu_S \tilde{\Gamma}^s + \beta^s \partial_s \beta^s, \tag{A5}$$

$$\partial_t \hat{K} = -\partial_s \partial_s \alpha + \beta^s \partial_s \hat{K}, \tag{A6}$$

$$\partial_t \tilde{A}_{ss} = \frac{\alpha}{3}\partial_s\partial_s\chi - \frac{\alpha}{3}\partial_s\partial_s\tilde{\gamma}_{ss} + \frac{\alpha}{6}\partial_s\partial_s\tilde{\gamma}_{qq} - \frac{2}{3}\chi\partial_s\partial_s\alpha + \frac{2}{3}\alpha\chi^2\partial_s\tilde{\Gamma}^s + \beta^s\partial_s\tilde{A}_{ss}, \tag{A7}$$

$$\partial_t \tilde{A}_{qq} = -\frac{\alpha}{3}\partial_s\partial_s\chi + \frac{\alpha}{3}\partial_s\partial_s\tilde{\gamma}_{ss} - \frac{\alpha}{6}\partial_s\partial_s\tilde{\gamma}_{qq} + \frac{2}{3}\chi\partial_s\partial_s\alpha - \frac{2}{3}\alpha\chi^2\partial_s\tilde{\Gamma}^s + \beta^s\partial_s\tilde{A}_{qq}, \tag{A8}$$

$$\partial_t \Theta = \frac{\alpha}{\chi}\partial_s\partial_s\chi - \frac{\alpha}{4\chi}\partial_s\partial_s\tilde{\gamma}_{ss} - \frac{\alpha}{4\chi}\partial_s\partial_s\tilde{\gamma}_{qq} + \frac{\alpha}{2}\chi\partial_s\tilde{\Gamma}^s + \beta^s\partial_s\Theta, \tag{A9}$$

$$\partial_t \tilde{\Gamma}^s = \frac{4}{3\chi}\partial_s\partial_s\beta^s - \frac{4\alpha}{3\chi}\partial_s\hat{K} - \frac{2\alpha}{3\chi}\partial_s\Theta + \beta^s\partial_s\tilde{\Gamma}^s, \tag{A10}$$

in the scalar sector,

$$\partial_t \tilde{\gamma}_{sA} = -2\alpha\tilde{A}_{sA} + \beta^s\partial_s\tilde{\gamma}_{sA}, \tag{A11}$$

$$\partial_t \beta^A = \alpha^2\mu_S\tilde{\Gamma}^A + \beta^s\partial_s\beta^A, \tag{A12}$$

$$\partial_t \tilde{A}_{sA} = -\frac{\alpha}{2\chi}\partial_s\partial_s\tilde{\gamma}_{sA} + \frac{\alpha}{2}\chi\partial_s\tilde{\Gamma}_A + \beta^s\partial_s\tilde{A}_{sA}, \tag{A13}$$

$$\partial_t \tilde{\Gamma}^A = \frac{1}{\chi}\partial_s\partial_s\beta^A + \beta^s\partial_s\tilde{\Gamma}^A, \tag{A14}$$

in the vector sector, and

$$\partial_t \tilde{\gamma}^{\mathrm{TF}}_{AB} = -2\alpha\tilde{A}^{\mathrm{TF}}_{AB} + \beta^s\partial_s\tilde{\gamma}^{\mathrm{TF}}_{AB}, \tag{A15}$$

$$\partial_t \tilde{A}^{\mathrm{TF}}_{AB} = -\frac{\alpha}{2}\partial_s\partial_s\tilde{\gamma}^{\mathrm{TF}}_{AB} + \beta^s\partial_s\tilde{A}^{\mathrm{TF}}_{AB}, \tag{A16}$$

in the tensor sector. Here the analysis is essentially for the linearized system, and we use the background metric γ_{ij} to raise and lower indices. We also use the convention that the spatial vector s^i is normalized to one against the background physical metric rather than using the conformal metric. The principal symbol of each sector can be trivially read off from these equations. In geometric units the tensor sector has speeds ± 1, and a complete set of characteristic variables. Likewise the vector sector has speeds $\pm(1, \sqrt{\bar{\mu}_S})$, with $\bar{\mu}_S = \mu_S/\chi$ and a complete set of characteristic variables. The scalar sector has speeds $0, \pm(1, \sqrt{\mu_L}, \sqrt{4\bar{\mu}_S/3})$, but does not have a full set of characteristic variables; the formulation is thus only weakly hyperbolic, and so does not have a well-posed initial value problem. It may be possible to modify the equations of motion by adding (possibly derivatives of) the algebraic constraints D and T to the equations of motion to achieve strong, or even symmetric hyperbolicity. But in any case it is not true that when the algebraic constraints are violated the PDE properties of the system are unaltered.

2. Numerical convergence without constraint projection

In the previous subsection we saw that when the algebraic constraints are not enforced, the Z4c formulation is only weakly hyperbolic. The open question is how ill posedness of the initial value problem will be reflected in numerical approximation. To answer the question we follow [50] and perform convergence tests, using the D_+ norm, as defined by (71), using initial data inspired by the robust stability test. Specifically we set the initial perturbation to $\epsilon \in (-10^{-3}/\rho^p, 10^{-3}/\rho^p)$. For the metric components we set $p = 3$, and use $p = 2$ for the remaining variables. This choice is needed to guarantee second order consistency of the initial data in the D_+ norm, which is of course necessary for convergence in that norm. We employ the same numerical grid used in the robust stability tests, but instead of evolving for of 1000 light-crossing times, we consider the interval $t \in [0, 0.8]$. We set the Courant factor to $\lambda = 0.5$, and use artificial dissipation (73) as usual with $\sigma = 0.02$. We consider higher resolutions than those used in the robust stability test, and compute additionally data with $\rho = 16, \ldots, 1024$, in factors of 2. Before calculating the D_+ norm, we restrict the solution to the $\rho = 1$ grid. The convergence factor with respect to resolutions ρ and 2ρ is

$$\mathcal{C} \equiv \log_2\left(\frac{\|u_\rho - u_{\mathrm{exact}}\|_{D_+}}{\|u_{2\rho} - u_{\mathrm{exact}}\|_{D_+}}\right). \tag{A17}$$

The convergence factors obtained with the puncture gauge condition (22) and (23) and the novel discretization are shown in Fig. 13. Very similar results are obtained with the standard discretization and we interpret the close agreement of the two tests as numerical evidence that the standard discretization is formally numerically stable, with constraint projection, despite our inability to prove so. At the lowest three resolutions the constraint projection does not seem to have any effect on the result, but at higher resolutions the conclusion is clear: without algebraic constraint projection the numerical solution does not converge to the continuum solution. Even with the constraint projection we do not seem to obtain perfect second order convergence, but since we are evolving random noise and the trend is clear, we conclude that with constraint projection the scheme is converging. Furthermore, in our tests with smooth initial data we do obtain perfect second order convergence with the constraint projection. We obtain similar results with a Courant factor $\lambda = 0.1$, and with the harmonic slicing and zero shift. We also find similar results when discretizing at fourth order.

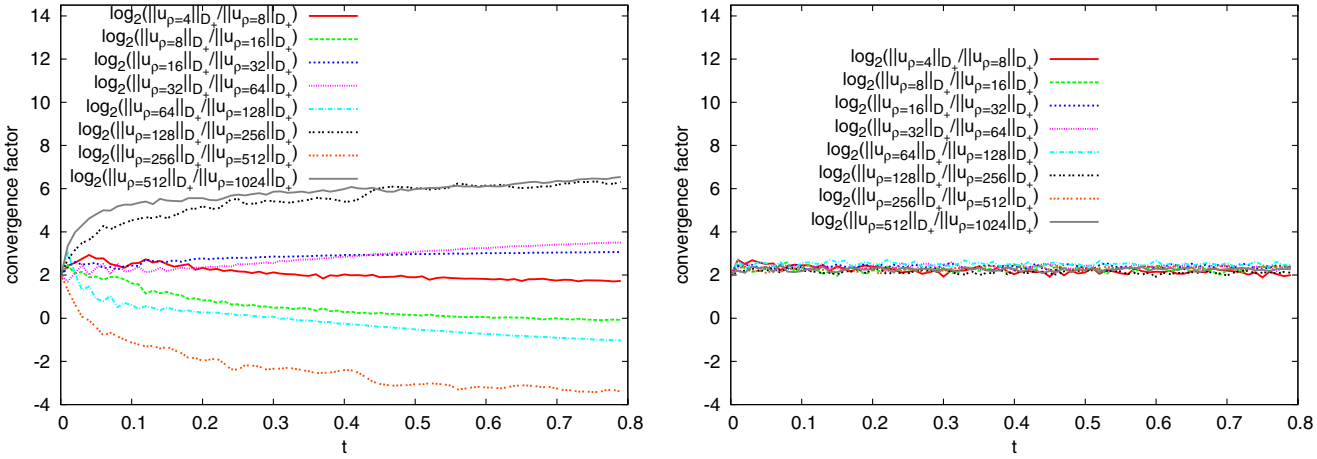

FIG. 13 (color online). Convergence test with the puncture gauge condition (22) and (23). Convergence factors (A17) in time for different resolution are shown. The left subplots are without algebra constraint enforcement while the right ones with. Here the novel finite-differencing scheme is used. Constraint projection is required for convergence.

APPENDIX B: SYMMETRIC HYPERBOLICITY OF Z4 WITH THE PUNCTURE GAUGE

1. Definitions

A quantity E conserved by the principal part of the second order system with state vector u,

$$E = \int \epsilon dx, \qquad \epsilon \equiv (\partial_j u, \partial_t u) H^{ij} (\partial_i u, \partial_t u)^\dagger, \tag{B1}$$

is called a candidate energy. The Hermitian matrix H is called a candidate symmetrizer. A system that admits a positive definite candidate symmetrizer is called symmetric hyperbolic. This definition is equivalent to the existence of a first order reduction of the system that is symmetric hyperbolic according to the standard definition for first order systems.

2. Z4c second order form

The principal part of the equations of motion of Z4c coupled to the puncture gauge can be written

$$\partial_0^2 \alpha = \mu_L \gamma^{ij} \partial_i \partial_j \alpha, \tag{B2}$$

$$\partial_0^2 \beta^i = \bar{\mu}_S \gamma^{jk} \partial_j \partial_k \beta^i + \frac{\bar{\mu}_S}{\mu_L} \partial^i \partial_0 \alpha + \frac{1}{6} \alpha \bar{\mu}_S \gamma^{jk} \partial^i \partial_0 \gamma_{jk}, \tag{B3}$$

$$\partial_0^2 \gamma_{ij} = \gamma^{kl} \partial_k \partial_l \gamma_{ij} + \frac{1}{3} \gamma^{kl} \partial_i \partial_j \gamma_{kl} + \frac{2}{\alpha} \partial_i \partial_j \alpha + \frac{2}{\alpha} \left(1 - \frac{1}{\bar{\mu}_S}\right) \gamma_{k(i} \partial_{j)} \partial_0 \beta^k, \tag{B4}$$

where we write $\partial_0 = (\partial_t - \beta^i \partial_i)/\alpha$. We thus express the principal part of the system in the form

$$\partial_0 u_{i\,kl} = \mathfrak{P}^{p}{}_{i}{}^{j}{}_{kl}{}^{mn} \partial_p u_{j\,mn}, \tag{B5}$$

with

$$\partial_0 u_{i\,kl} = (\partial_i \gamma_{kl}, \partial_i \alpha, \partial_i \beta_k, \partial_0 \gamma_{kl}, \partial_0 \alpha, \partial_0 \beta_k)^\dagger, \tag{B6}$$

and the principal part matrix given by

$$\mathfrak{P}^{p}{}_{i}{}^{j}{}_{kl}{}^{mn} \partial_p u_{jmn} = \begin{pmatrix} 0 & \delta^p{}_i I_{kl}{}^{mn} \\ \mathcal{A}^{pj}{}_{kl}{}^{mn} & \mathcal{B}^{p}{}_{kl}{}^{mn} \end{pmatrix}, \tag{B7}$$

with $I_{kl}{}^{mn}$ the appropriate identity and

$$\mathcal{A}^{pj}{}_{kl}{}^{mn} = \begin{pmatrix} \mathcal{A}^{pj}{}_{11\,kl}{}^{mn} & \frac{2}{\alpha} \delta^p{}_{(k} \delta^j{}_{l)} & 0 \\ 0 & \mu_L \gamma^{pj} & 0 \\ 0 & 0 & \bar{\mu}_S \gamma^{pj} \delta^k{}_m \end{pmatrix}, \tag{B8}$$

$$\mathcal{B}^{p}{}_{kl}{}^{mn} = \begin{pmatrix} 0 & 0 & \frac{2}{\alpha}\left(1 - \frac{1}{\bar{\mu}_S}\right) \delta^p{}_{(k} \gamma_{l)m} \\ 0 & 0 & 0 \\ \frac{\alpha}{6} \bar{\mu}_S \gamma^{mn} \gamma^{pk} & \frac{\bar{\mu}_S}{\mu_L} \gamma^{pk} & 0 \end{pmatrix}, \tag{B9}$$

where

$$\mathcal{A}^{\,pj}_{11\,kl}{}^{mn} = \gamma^{pj} \delta^m{}_{(k} \delta^n{}_{l)} + \tfrac{1}{3} \gamma^{mn} \delta^p{}_{(k} \delta^j{}_{l)}. \tag{B10}$$

3. Ansatz candidate and conservation

Starting from the ansatz candidate [55],

$$H^{ijklmn} = \begin{pmatrix} H_{11}^{ijklmn} & H_{12}^{ijkl} & 0 & 0 & 0 & H_{16}^{iklm} \\ H_{12}^{jimn} & H_{22}^{ij} & 0 & 0 & 0 & H_{26}^{im} \\ 0 & 0 & H_{33}^{ijkm} & H_{34}^{ikmn} & H_{35}^{ik} & 0 \\ 0 & 0 & H_{34}^{jmkl} & H_{44}^{klmn} & H_{45}^{kl} & 0 \\ 0 & 0 & H_{35}^{jm} & H_{45}^{mn} & H_{55} & 0 \\ H_{16}^{jmnk} & H_{26}^{jk} & 0 & 0 & 0 & H_{66}^{km} \end{pmatrix}, \quad \text{(B11)}$$

where we define

$$\begin{aligned} H_{11}^{ijklmn} &= H_{11}^1 \gamma^{ij}\gamma^{kl}\gamma^{mn} + 2H_{11}^2 \gamma^{ij}\gamma^{k(m}\gamma^{n)l} \\ &\quad + 2H_{11}^3(\gamma^{i(k}\gamma^{l)j}\gamma^{mn} + \gamma^{i(m}\gamma^{n)j}\gamma^{kl}) \\ &\quad + 2H_{11}^4(\gamma^{ik}\gamma^{j(m}\gamma^{n)l} + \gamma^{il}\gamma^{j(m}\gamma^{n)k} \\ &\quad + \gamma^{im}\gamma^{j(k}\gamma^{l)n} + \gamma^{in}\gamma^{j(k}\gamma^{l)m}) \\ &\quad + A_{11}^1(\gamma^{k[i}\gamma^{j]}{}^{(m}\gamma^{n)l} + \gamma^{l[i}\gamma^{j]}{}^{(m}\gamma^{n)m}), \\ H_{12}^{ijkl} &= 2H_{12}^1 \gamma^{i(k}\gamma^{l)j} + H_{12}^2 \gamma^{ij}\gamma^{kl}, \\ H_{22}^{ij} &= H_{22}^1 \gamma^{ij}, \\ H_{33}^{ijkm} &= 2H_{33}^1 \gamma^{i(k}\gamma^{m)j} + H_{33}^2 \gamma^{ij}\gamma^{km} + A_{33}^1 \gamma^{k[i}\gamma^{j]m}, \\ H_{16}^{iklm} &= 2H_{16}^1 \gamma^{i(k}\gamma^{l)m} + H_{16}^2 \gamma^{im}\gamma^{kl}, \\ H_{26}^{im} &= H_{26}^1 \gamma^{im}, \\ H_{34}^{ikmn} &= H_{34}^1 \gamma^{i(m}\gamma^{n)k} + H_{34}^2 \gamma^{ik}\gamma^{mn}, \\ H_{35}^{ik} &= H_{35}^1 \gamma^{ik}, \\ H_{44}^{klmn} &= 2H_{44}^1 \gamma^{k(m}\gamma^{n)l} + H_{44}^2 \gamma^{kl}\gamma^{mn}, \\ H_{45}^{kl} &= H_{45}^1 \gamma^{kl}, \\ H_{66}^{km} &= H_{66}^1 \gamma^{km}. \end{aligned}$$

Because of the structure of the equations of motion and our choice of gauge the block structure of the ansatz candidate is no restriction. The restriction to energy densities constructed by using the metric to construct indices does restrict the class of symmetrizers, but is the largest natural choice. Conservation of the energy is guaranteed by Hermiticity of the matrix, suppressing nonderivative indices,

$$S_i H^{ij} \mathfrak{Y}\{^p{}_j{}^k s_p S_k, \quad \text{(B12)}$$

for every spatial vector s^i, where

$$S_i = \begin{pmatrix} s_i & 0 \\ 0 & 1 \end{pmatrix}, \quad \text{(B13)}$$

and the partition of this matrix is compatible with that of $u_{i\,kl}$ into spatial and time derivatives. Imposing energy conservation for the puncture gauge implies that

$$\begin{aligned} H_{11}^1 &= \frac{2}{9}(6H_{44}^2 - \alpha H_{34}^2), & H_{11}^2 &= 0, \\ H_{11}^3 &= 0, & H_{11}^4 &= 0, \\ H_{12}^1 &= 0, & H_{16}^1 &= 0, \\ H_{16}^2 &= \frac{4}{3\bar{\mu}_S} H_{34}^2, & H_{33}^1 &= \frac{1-\bar{\mu}_S}{\bar{\mu}_S \alpha} H_{34}^2, \\ H_{34}^1 &= 0, & H_{44}^1 &= 0, \end{aligned}$$

and the more complicated

$$\begin{aligned} H_{22}^1 &= \mu_L H_{55} + \frac{8H_{34}^2(2\bar{\mu}_S - 3)}{\mu_L(3\mu_L - 4\bar{\mu}_S)\alpha} \\ &\quad - \frac{12H_{44}^2(4 + \mu_L - 4\bar{\mu}_S}{\mu_L(3\mu_L - 4\bar{\mu}_S)\alpha^2}, \\ H_{26}^1 &= \frac{24(\bar{\mu}_S - 1)}{\bar{\mu}_S(4\bar{\mu}_S - 3\mu_L)}(2H_{44}^2 + \alpha H_{34}^2), \\ H_{35}^1 &= \frac{24 - 6\mu_L - 16\bar{\mu}_S}{\mu_L(3\mu_L - 4\bar{\mu}_S)\alpha} H_{34}^2 + \frac{48(\bar{\mu}_S - 1)}{\mu_L(4\bar{\mu}_S - 3\mu_L)\alpha^2} H_{44}^2, \\ H_{45}^1 &= \frac{4\bar{\mu}_S}{\mu_L(4\bar{\mu}_S - 3\mu_L)} H_{34}^2 + \frac{6}{4\bar{\mu}_S - 3\mu_L} H_{44}^2, \\ H_{66}^1 &= \frac{2(3\bar{\mu}_S - 4)}{\bar{\mu}_S^2 \alpha} H_{34}^2 + \frac{12(\bar{\mu}_S - 1)}{\bar{\mu}_S^2 \alpha^2} H_{44}^2, \\ H_{12}^2 &= \frac{4}{4\bar{\mu}_S - 3\mu_L} H_{34}^2 + \frac{8}{(4\bar{\mu}_S - 3\mu_L)\alpha} H_{44}^2, \\ H_{33}^2 &= \frac{2(3\bar{\mu}_S - 4)}{\bar{\mu}_S \alpha} H_{34}^2 + \frac{12(\bar{\mu}_S - 1)}{\bar{\mu}_S \alpha^2} H_{44}^2, \end{aligned}$$

Note that the terms antisymmetric in derivative indices drop out of the conservation equations.

4. Positivity

Introducing and expanding with a tensor basis reveals vanishing elements on the diagonal of the candidate symmetrizer; there is no positive definite candidate symmetrizer starting from the natural ansatz (B11). We thus conclude, unfortunately, that the use of summation by parts finite differences for the Z4c formulation with the puncture gauge will not guarantee numerical stability.

[1] F. Pretorius, Classical Quantum Gravity **22**, 425 (2005).
[2] F. Pretorius, Phys. Rev. Lett. **95**, 121101 (2005).
[3] L. Lindblom, M. A. Scheel, L. E. Kidder, R. Owen, and O. Rinne, Classical Quantum Gravity **23**, S447 (2006).
[4] C. Palenzuela, I. Olabarrieta, L. Lehner, and S. L. Liebling, Phys. Rev. D **75**, 064005 (2007).
[5] B. Szilágyi, D. Pollney, L. Rezzolla, J. Thornburg, and J. Winicour, Classical Quantum Gravity **24**, S275 (2007).
[6] H. Friedrich, Commun. Math. Phys. **100**, 525 (1985).
[7] D. Garfinkle, Phys. Rev. D **65**, 044029 (2002).
[8] B. Szilágyi and J. Winicour, Phys. Rev. D **68**, 041501 (2003).
[9] H.-O. Kreiss and J. Winicour, Classical Quantum Gravity **23**, S405 (2006).
[10] M. C. Babiuc, B. Szilágyi, and J. Winicour, Phys. Rev. D **73**, 064017 (2006).
[11] M. Motamed, M. C. Babiuc, B. Szilagyi, H.-O. Kreiss, and J. Winicour, Phys. Rev. D **73**, 124008 (2006).
[12] O. Rinne, Classical Quantum Gravity **23**, 6275 (2006).
[13] M. Ruiz, O. Rinne, and O. Sarbach, Classical Quantum Gravity **24**, 6349 (2007).
[14] O. Rinne, L. T. Buchman, M. A. Scheel, and H. P. Pfeiffer, Classical Quantum Gravity **26**, 075009 (2009).
[15] C. Gundlach, J. M. Martin-Garcia, G. Calabrese, and I. Hinder, Classical Quantum Gravity **22**, 3767 (2005).
[16] T. W. Baumgarte and S. L. Shapiro, Phys. Rev. D **59**, 024007 (1998).
[17] M. Shibata and T. Nakamura, Phys. Rev. D **52**, 5428 (1995).
[18] T. Nakamura, K. Oohara, and Y. Kojima, Prog. Theor. Phys. Suppl. **90**, 1 (1987).
[19] J. G. Baker, J. Centrella, D.-I. Choi, M. Koppitz, and J. van Meter, Phys. Rev. Lett. **96**, 111102 (2006).
[20] M. Campanelli, C. O. Lousto, P. Marronetti, and Y. Zlochower, Phys. Rev. Lett. **96**, 111101 (2006).
[21] U. Sperhake, V. Cardoso, F. Pretorius, E. Berti, and J. A. González, Phys. Rev. Lett. **101**, 161101 (2008).
[22] U. Sperhake, V. Cardoso, F. Pretorius, E. Berti, T. Hinderer, and N. Yunes, Phys. Rev. Lett. **103**, 131102 (2009).
[23] C. Gundlach and J. M. Martin-Garcia, Phys. Rev. D **74**, 024016 (2006).
[24] D. Nunez and O. Sarbach, Phys. Rev. D **81**, 044011 (2010).
[25] S. Bernuzzi and D. Hilditch, Phys. Rev. D **81**, 084003 (2010).
[26] C. Bona, T. Ledvinka, C. Palenzuela, and M. Žáček, Phys. Rev. D **67**, 104005 (2003).
[27] C. Bona and C. Palenzuela, Phys. Rev. D **69**, 104003 (2004).
[28] C. Bona, T. Ledvinka, C. Palenzuela, and M. Žáček, Phys. Rev. D **69**, 064036 (2004).
[29] C. Bona, T. Ledvinka, C. Palenzuela-Luque, and M. Zacek, Classical Quantum Gravity **22**, 2615 (2005).
[30] D. Alic, C. Bona, and C. Bona-Casas, Phys. Rev. D **79**, 044026 (2009).
[31] C. Bona, C. Bona-Casas, and C. Palenzuela, Phys. Rev. D **82**, 124010 (2010).
[32] C. Bona and C. Bona-Casas, Phys. Rev. D **82**, 064008 (2010).
[33] M. Ruiz, D. Hilditch, and S. Bernuzzi, Phys. Rev. D **83**, 024025 (2011).
[34] A. Weyhausen, S. Bernuzzi, and D. Hilditch, Phys. Rev. D **85**, 024038 (2012).
[35] D. Alic, C. Bona-Casas, C. Bona, L. Rezzolla, and C. Palenzuela, Phys. Rev. D **85**, 064040 (2012).
[36] C. Bona, J. Massó, E. Seidel, and J. Stela, Phys. Rev. Lett. **75**, 600 (1995).
[37] M. Alcubierre, B. Brügmann, P. Diener, M. Koppitz, D. Pollney, E. Seidel, and R. Takahashi, Phys. Rev. D **67**, 084023 (2003).
[38] G. Calabrese, I. Hinder, and S. Husa, J. Comput. Phys. **218**, 607 (2006).
[39] M. Chirvasa and S. Husa, J. Comput. Phys. **229**, 2675 (2010).
[40] H. Witek, D. Hilditch, and U. Sperhake, Phys. Rev. D **83**, 104041 (2011).
[41] H. O. Kreiss and J. Lorenz, *Initial-Boundary Value Problems and the Navier-Stokes Equations* (Academic Press, New York, 1989).
[42] B. Gustafsson, H.-O. Kreiss, and J. Oliger, *Time Dependent Problems and Difference Methods* (Wiley, New York, 1995).
[43] A. M. Knapp, E. J. Walker, and T. W. Baumgarte, Phys. Rev. D **65**, 064031 (2002).
[44] G. Nagy, O. E. Ortiz, and O. A. Reula, Phys. Rev. D **70**, 044012 (2004).
[45] Z.-j. Cao, H.-J. Yo, and J.-P. Yu, Phys. Rev. D **78**, 124011 (2008).
[46] P. Galaviz, B. Brügmann, and Z. Cao, Phys. Rev. D **82**, 024005 (2010).
[47] Z. Cao and C. Liu, Int. J. Mod. Phys. D **20**, 43 (2011).
[48] M. Alcubierre, G. Allen, C. Bona, D. Fiske, T. Goodale, F. S. Guzmán, I. Hawke, S. H. Hawley, S. Husa, M. Koppitz *et al.*, Classical Quantum Gravity **21**, 589 (2004).
[49] M. C. Babiuc, S. Husa, D. Alic, I. Hinder, C. Lechner, E. Schnetter, B. Szilagyi, Y. Zlochower, N. Dorband, D. Pollney *et al.*, Classical Quantum Gravity **25**, 125012 (2008).
[50] I. Hinder, Ph.D. thesis, School of Mathematics, University of Southampton (2005).
[51] M. Boyle, L. Lindblom, H. Pfeiffer, M. Scheel, and L. E. Kidder, Phys. Rev. D **75**, 024006 (2007).
[52] W. Tichy, Phys. Rev. D **80**, 104034 (2009).
[53] V. Paschalidis, J. Hansen, and A. Khokhlov, Phys. Rev. D **78**, 064048 (2008).
[54] C. Gundlach and J. M. Martin-Garcia, Classical Quantum Gravity **23**, S387 (2006).
[55] D. Hilditch and R. Richter, arXiv:1002.4119.